Cell

Inverse Synaptic Tagging of Inactive Synapses via Dynamic Interaction of Arc/Arg3.1 with CaMKIIβ

Hiroyuki Okuno,[1,6,*] Kaori Akashi,[3] Yuichiro Ishii,[1,2] Nan Yagishita-Kyo,[1,2] Kanzo Suzuki,[1,2] Mio Nonaka,[1,2,6] Takashi Kawashima,[1,2] Hajime Fujii,[1,6] Sayaka Takemoto-Kimura,[1,4] Manabu Abe,[3] Rie Natsume,[3] Shoaib Chowdhury,[5] Kenji Sakimura,[3,6] Paul F. Worley,[5] and Haruhiko Bito[1,2,6,*]

[1]Department of Neurochemistry
[2]Global Center of Education and Research for Chemical Biology of the Diseases
Graduate School of Medicine, The University of Tokyo, Bunkyo-ku, Tokyo 113-0033, Japan
[3]Department of Cellular Neurobiology, Brain Research Institute, Niigata University, Niigata 951-8585, Japan
[4]PRESTO-JST, Kawaguchi, Saitama 332-0012, Japan
[5]Department of Neuroscience, Johns Hopkins University School of Medicine, Baltimore, MD 21205, USA
[6]CREST-JST, Chiyoda-ku, Tokyo 102-0076, Japan
*Correspondence: okuno@m.u-tokyo.ac.jp (H.O.), hbito@m.u-tokyo.ac.jp (H.B.)
DOI 10.1016/j.cell.2012.02.062

SUMMARY

The Arc/Arg3.1 gene product is rapidly upregulated by strong synaptic activity and critically contributes to weakening synapses by promoting AMPA-R endocytosis. However, how activity-induced Arc is redistributed and determines the synapses to be weakened remains unclear. Here, we show targeting of Arc to inactive synapses via a high-affinity interaction with CaMKIIβ that is not bound to calmodulin. Synaptic Arc accumulates in inactive synapses that previously experienced strong activation and correlates with removal of surface GluA1 from individual synapses. A lack of CaMKIIβ either in vitro or in vivo resulted in loss of Arc upregulation in the silenced synapses. The discovery of Arc's role in "inverse" synaptic tagging that is specific for weaker synapses and prevents undesired enhancement of weak synapses in potentiated neurons reconciles essential roles of Arc both for the late phase of long-term plasticity and for reduction of surface AMPA-Rs in stimulated neurons.

INTRODUCTION

An outstanding challenge in neuroscience is the identification and characterization of neuronal activity-regulated genes that critically govern the molecular and cellular events underlying memory formation and processing (Bito et al., 1996; Flavell et al., 2006; Nedivi et al., 1993; Qian et al., 1993; Worley et al., 1993). The neuronal immediate early gene *Arc* (also called *Arg*3.1) is among the most promising candidates for such memory regulatory genes because it is dynamically regulated, and its induction highly correlates with augmented neuronal activity that is required for cognitive processes such as spatial learning and memory consolidation (Guzowski et al., 1999; Link et al., 1995; Lyford et al., 1995; Ramírez-Amaya et al., 2005). Consistent with such an activity-dependent *Arc* upregulation, the knockdown or knockout (KO) of *Arc* in rodents causes impairments in the persistence of long-term memory (Guzowski et al., 2000; Plath et al., 2006; Ploski et al., 2008) and in stimulus selectivity or experience-dependent cortical plasticity in the visual cortex (McCurry et al., 2010; Wang et al., 2006).

A large part of *Arc* function occurs postsynaptically. Biochemical and electron microscopy (EM) studies showed presence of Arc protein in the postsynaptic density (PSD) of activated neurons (Chowdhury et al., 2006; Moga et al., 2004). In the PSD, Arc interacts with the endocytic proteins endophilin and dynamin and enhances the removal of AMPA-type glutamate receptors (AMPA-Rs) from the postsynaptic membrane (Chowdhury et al., 2006). This function, together with the activity-dependent expression of *Arc*, is implicated in several forms of protein translation-dependent synaptic long-term depression (LTD) (Park et al., 2008; Plath et al., 2006; Smith-Hicks et al., 2010; Waung et al., 2008) and homeostatic plasticity/synaptic scaling (Béïque et al., 2011; Chowdhury et al., 2006; Peebles et al., 2010; Rial Verde et al., 2006; Shepherd et al., 2006). This role of *Arc* in the cell-wide weakening of glutamatergic synaptic strength, however, is difficult to reconcile with a large amount of evidence that *Arc* is most strongly induced by stimuli that evoke long-term potentiation (LTP) (Link et al., 1995; Messaoudi et al., 2007; Moga et al., 2004; Ying et al., 2002) and that both *Arc* mRNA and protein accumulate in the dendritic areas that receive high-frequency synaptic inputs (Moga et al., 2004; Steward et al., 1998). Such incongruity still remains because we critically lack knowledge about the molecular mechanisms of Arc association with PSD regions.

In this study, we have investigated the potential role of CaMKIIβ in determining the targeting of synaptic activity-induced Arc protein from the soma to individual synapses and

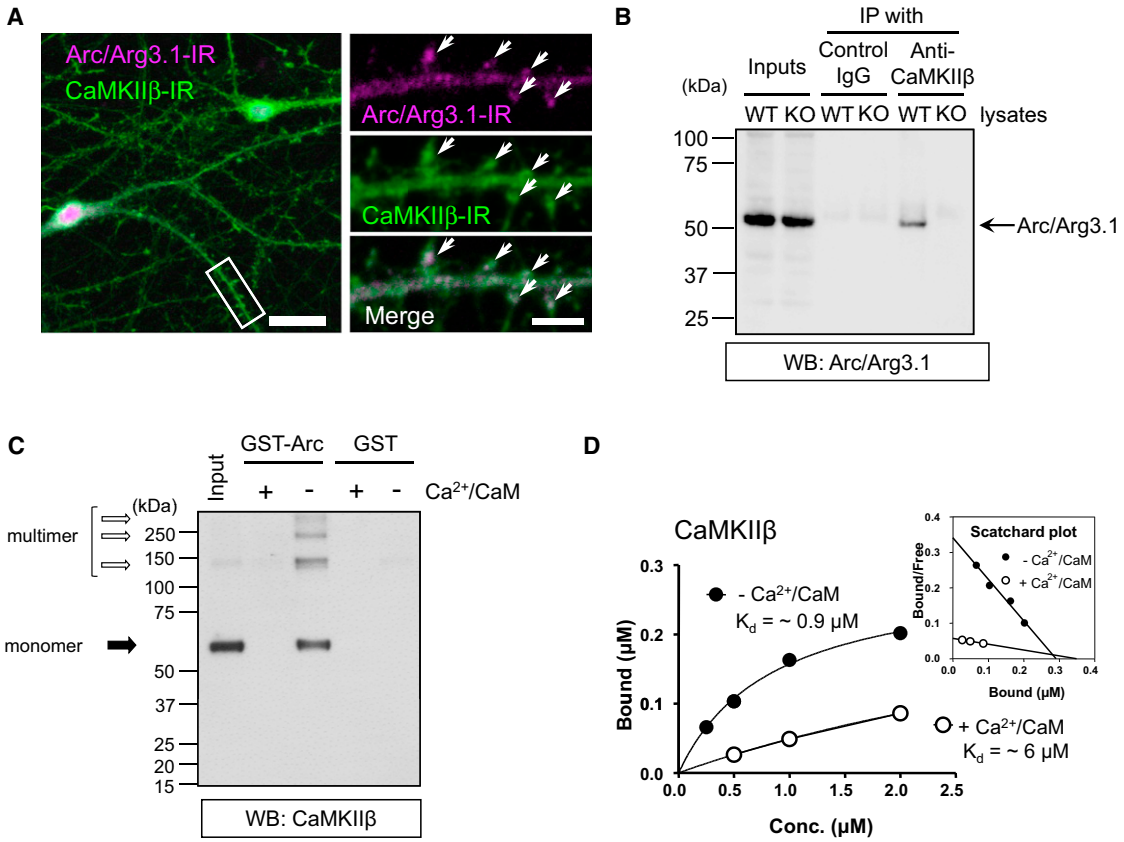

Figure 1. Arc Interacts with CaMKIIβ

(A) Colocalization of Arc with CaMKIIβ in dendritic spines is shown. A dendritic segment of a representative cell (left) is expanded and shown in a frame (right). Arrows represent spines containing both Arc-IR and CaMKIIβ-IR. Scale bars, 20 μm (left) and 5 μm (right).

(B) Coimmunoprecipitation of Arc and CaMKIIβ in brain synaptosomal fractions. IP, immunoprecipitation; WB, western blot.

(C) GST pull-down experiments reveal a stringent calcium dependency for Arc-CaMKIIβ binding, which was suppressed when both Ca^{2+} and CaM were present.

(D) Scatchard analysis confirms strong binding of Arc to CaM-unbound CaMKIIβ (− Ca^{2+}/CaM) and a reduced binding upon CaMKIIβ activation (+ Ca^{2+}/CaM). Conc., concentration.

See also Figure S1.

demonstrate an "inverse synaptic tagging" mechanism whereby an interaction between Arc and CaMKIIβ operates as a specific sensor that mediates the inactive synapse-specific control of AMPA-R clearance at weaker synapses in potentiated neurons, based on a local history of both activity and inactivity.

RESULTS

Arc Directly Interacts with CaMKIIβ in Dendritic Spines

A yeast two-hybrid screen was carried out to isolate putative postsynaptic Arc-binding proteins (Chowdhury et al., 2006). The screening yielded the β-isoform of CaMKII (CaMKIIβ) as a binding partner candidate, and this binding was confirmed by an in vitro coimmunoprecipitation assay (Figure S1A available online). In hippocampal CA1/CA3 cell cultures, Arc immunoreactivity (IR) colocalized with CaMKIIβ IR in the dendritic spines of Arc-expressing neurons (Figure 1A). Furthermore, Arc IR was immunoprecipitated with an anti-CaMKIIβ antibody in brain lysates from wild-type (WT), but not from CaMKIIβ-KO, mice (Figures 1B and S1B), indicating that Arc and CaMKIIβ are complexed in the brain. Arc-CaMKIIβ association was further tested in situ, using fluorescence resonance energy transfer (FRET) between CFP-tagged Arc (Arc-CFP) and YFP-tagged CaMKIIβ (CaMKIIβ-YFP). Arc-CFP showed a significant FRET with CaMKIIβ-YFP in spines of living hippocampal neurons treated with tetrodotoxin (TTX) ($p < 0.0001$; Figure S1C), but not with other tagged PSD proteins, such as CaMKIIα-YFP and Homer1c-YFP, suggesting a high specificity for Arc-CaMKIIβ interaction.

High-Affinity Arc-CaMKIIβ Binding in the Absence of Ca^{2+} and Its Suppression by Ca^{2+}/CaM

We next investigated the biochemical properties of Arc-CaMKIIβ interaction. A GST pull-down experiment confirmed direct binding between recombinant Arc and CaMKIIβ. This interaction was strong in the absence of Ca^{2+} and calmodulin (CaM) but was attenuated when Ca^{2+}/CaM was present (Figures 1C and S1D). In contrast, an Arc-CaMKIIα interaction was observed only in

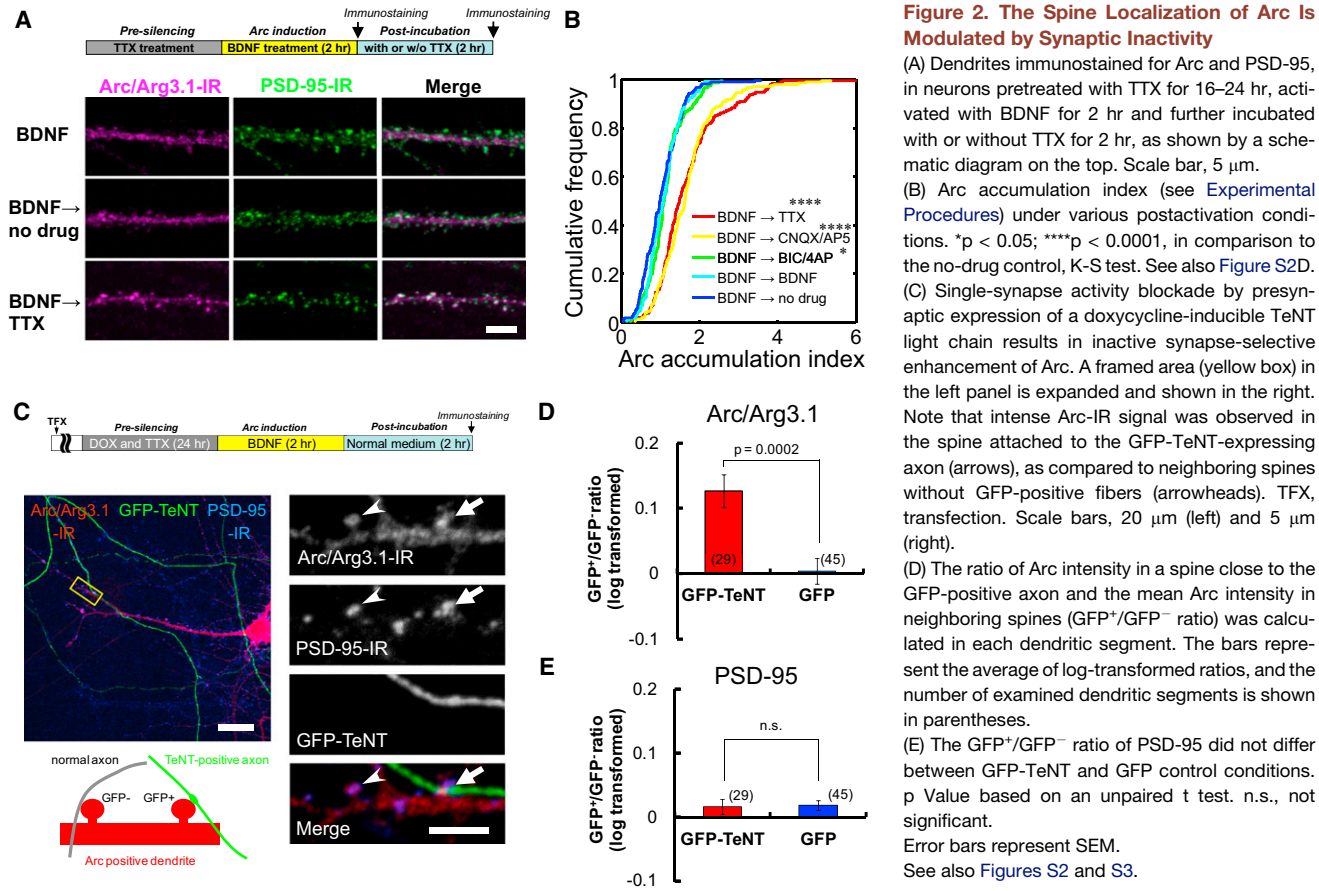

Figure 2. The Spine Localization of Arc Is Modulated by Synaptic Inactivity

(A) Dendrites immunostained for Arc and PSD-95, in neurons pretreated with TTX for 16–24 hr, activated with BDNF for 2 hr and further incubated with or without TTX for 2 hr, as shown by a schematic diagram on the top. Scale bar, 5 μm.

(B) Arc accumulation index (see Experimental Procedures) under various postactivation conditions. *p < 0.05; ****p < 0.0001, in comparison to the no-drug control, K-S test. See also Figure S2D.

(C) Single-synapse activity blockade by presynaptic expression of a doxycycline-inducible TeNT light chain results in inactive synapse-selective enhancement of Arc. A framed area (yellow box) in the left panel is expanded and shown in the right. Note that intense Arc-IR signal was observed in the spine attached to the GFP-TeNT-expressing axon (arrows), as compared to neighboring spines without GFP-positive fibers (arrowheads). TFX, transfection. Scale bars, 20 μm (left) and 5 μm (right).

(D) The ratio of Arc intensity in a spine close to the GFP-positive axon and the mean Arc intensity in neighboring spines (GFP^+/GFP^- ratio) was calculated in each dendritic segment. The bars represent the average of log-transformed ratios, and the number of examined dendritic segments is shown in parentheses.

(E) The GFP^+/GFP^- ratio of PSD-95 did not differ between GFP-TeNT and GFP control conditions. p Value based on an unpaired t test. n.s., not significant.

Error bars represent SEM.

See also Figures S2 and S3.

the presence of Ca^{2+}/CaM (Figure S1E). The CaM-binding inhibitor W-7 reversed the effects of Ca^{2+}/CaM (Figure S1F). Based on Scatchard analyses, the measured affinity between Arc and CaMKIIβ was indeed high (~0.9 μM) in the absence of Ca^{2+}/CaM; it decreased by 7-fold in the presence of Ca^{2+}/CaM (K_d, ~6 μM) (Figure 1D). In contrast, Arc-CaMKIIα interactions showed a much lower affinity (K_d, ~10 μM with Ca^{2+}/CaM; ~60 μM without Ca^{2+}/CaM) (data not shown). These results, together, suggested that Arc preferentially binds to CaMKIIβ in a Ca^{2+}/CaM-unbound, inactive, state.

Arc Is More Enriched in the PSD during Synaptic Inactivity following De Novo Transcription-Inducing Stimuli in Cultured Neurons

This interaction raised the possibility that Arc synaptic localization could be regulated by synaptic activity and inactivity through modulation of Ca^{2+}/CaM binding to CaMKIIβ. We directly tested this, by application of de novo transcription-inducing stimuli and then monitoring newly synthesized Arc protein at the PSD, after maintaining or shutting down synaptic activity. Cultured hippocampal CA1/CA3 neurons were pretreated with TTX until pre-existing Arc protein was cleared (Figure S2A) and then stimulated by BDNF application for 2 hr, similar to a protocol that has been shown to induce strong CA1-LTP accompanied by new *Arc* induction (Ying et al., 2002). Immediately after BDNF activation, new synthesis of Arc protein was strongly induced (Figures S2A–S2C). Arc IR was mainly associated with the dendritic shaft, although a minority was present in the PSD (Figure 2A, BDNF). Additional incubation with a basal medium caused little change in Arc localization (Figure 2A, BDNF → no drug). However, when spontaneous synaptic activity was blocked with TTX after the BDNF treatment, Arc IR intensity in the PSD became much more pronounced (Figure 2A, BDNF → TTX). Although surprising and counterintuitive, this finding was in accordance with the biochemical-binding data that favored Arc association with inactive CaMKIIβ. To compare data across different conditions, we calculated an Arc accumulation index by normalizing spine Arc expression levels to the adjacent dendritic shafts (see Experimental Procedures). Based on this index, we found little change between "no drug after BDNF" and "BDNF after BDNF" conditions (Figure 2B, BDNF → no drug and BDNF → BDNF). In contrast, either "BDNF → TTX" or "BDNF → CNQX/AP5" treatment, which inhibits glutamatergic transmission pre- or postsynaptically, caused a significant rightward shift in the synaptic Arc distribution (Figure 2B; p < 0.0001, Kolmogorov-Smirnov [K-S] test). Enhancing glutamatergic synaptic activity using a cocktail of the $GABA_A$ receptor antagonist bicuculline and a presynaptic potassium-channel blocker, 4-aminopyridine, had little effect (Figure 2B, BDNF → BIC/4AP). Consistent with these results, after activity blockade, the absolute Arc IR was enriched in the

PSD, whereas the shaft IR decreased, thus creating an Arc gradient that favored synaptic Arc (Figure S2D). Consistent with this sensitivity to inactivity, Arc IR intensity exhibited a significantly higher coefficient of variation in individual PSDs of neurons expressing Arc under a basal medium condition, compared to that of another PSD protein, Homer (Figure S2E). Taken together, these results pointed to the surprising possibility that perhaps individual history of synaptic inactivity, but not enhanced activity, contributed to the synaptic pool of newly induced Arc protein.

Essentially similar results were obtained using neuronal cultures of hippocampal dentate gyrus (DG), which is known to express the highest amounts of activity-induced *Arc* mRNA and proteins (Link et al., 1995; Lyford et al., 1995; Steward et al., 1998). BIC/4AP treatment for 2 hr induced strong expression of newly translated Arc in our DG neuron culture (Figure S3A), and a subsequent follow-up treatment with TTX for an additional 2 hr (BIC/4AP → TTX 2 hr; $p < 0.0001$, K-S test), but not with BIC/4AP (BIC/4AP 4 hr), caused an increase in synaptic Arc (Figures S3B and S3C). This inactivity-induced enrichment was further promoted when TTX duration was extended to 4 hr ($p < 0.001$, K-S test for BIC/4AP 2 hr → TTX 2 hr versus BIC/4AP 2 hr → TTX 4 hr), whereas BIC/4AP follow-up for 4 hr (BIC/4AP 6 hr) had little effect (Figure S3B). In contrast, no such enrichment was observed for PSD-95 (data not shown).

Increased Synaptic Arc Maintenance Is Induced by Single-Synapse Inactivation

To discriminate whether Arc protein dynamics reflected the degree of local synaptic inactivity of individual synapses rather than the degree of general, cell-wide activity or inactivity, we suppressed synaptic activity on a single-synapse basis by expressing doxycycline-inducible GFP-tagged tetanus toxin (GFP-TeNT) presynaptically, resulting in cleavage of VAMP2 and blocking neurotransmitter release in the GFP-labeled axon (Figure 2C) (Yamamoto et al., 2003). To ensure scoring of the effect of TeNT on excitatory, but not inhibitory, synapses, BDNF-induced Arc IR was measured only in PSD-95 containing dendritic spines in hippocampal CA1/CA3 neurons. The Arc IR at spines contacting GFP-TeNT-positive axons was significantly higher than those at adjacent spines that were juxtaposed to GFP-TeNT-negative boutons (Figures 2C and 2D). Such an inactive synapse-restricted regulation was not observed for PSD-95 IR (Figure 2E). Similar results were obtained using DG granule cells activated with BIC/4AP (Figure S3D). Local synaptic inactivity thus directly controls spine Arc dynamics in a synapse-autonomous manner.

Time-Lapse Imaging of Synaptic Accumulation of Arc during Inactivity

To examine the single-spine kinetics of Arc dynamics exposed to synaptic inactivity after Arc induction, we developed a live Arc protein reporter-imaging system in which activity-dependent expression and synaptic targeting of Arc protein were monitored over time in the same dendritic spines. A monomeric EGFP-tagged Arc (mEGFP-Arc) was driven under the control of the 7 kb *Arc* promoter (Kawashima et al., 2009) in hippocampal neurons along with a volume-filling RFP that was constitutively expressed. The initial mEGFP-Arc distribution after a 2 hr BDNF treatment recapitulated the distribution of endogenous Arc IR; the mEGFP-Arc signals were mainly observed in the dendritic shafts, and minor pools of the signal were detected in some spines (Figure 3A, left panels; also see Figure 2A). We found that mEGFP-Arc signals accumulated more in dendritic spines than in shafts after cessation of activity in TTX (Figure 3A, upper panels), but not when spontaneous activity remained (Figure 3A, lower panels). Volume-normalized mEGFP-Arc intensity in individual spines also revealed significant increases over time during synaptic inactivity (Figure 3B) ($p < 0.003$, K-S test). We further carried out dual-color live imaging of constitutively expressed mEGFP-tagged CaMKIIβ (mEGFP-CaMKIIβ) and activity-driven mCherry-tagged Arc (mCherry-Arc) (Figure 3C). We chose an experimental condition under which BDNF 2 hr treatment strongly induced new expression of mCherry-Arc from the *Arc* 7 kb promoter while it evoked little dynamic translocation of mEGFP-CaMKIIβ (Figures 3C and 3D). Interestingly, ensemble data revealed that at 2 hr after TTX treatment, the quantity of spine mCherry-Arc during TTX treatment positively correlated with that of spine mEGFP-CaMKIIβ, but not at 30 min after BDNF treatment (Figure 3E). This suggested that Arc accumulation in a spine during a period of inactivity might be determined by the CaMKIIβ level in the spine at the start of the inactivity period.

Effects of Inactivity-Enhanced Arc Synaptic Localization on GluA1 Surface Expression

Previous studies showed that Arc interacted with the endocytic machinery and regulated the trafficking of the GluA1 subunit of AMPA-R (Béïque et al., 2011; Chowdhury et al., 2006; Rial Verde et al., 2006; Shepherd et al., 2006). Consequently, we examined whether preferential Arc maintenance at individual inactive postsynapses may help control GluA1 surface expression levels (Figure 4).

When hippocampal CA1/CA3 neurons were treated with BDNF for 2 hr, surface expression levels of synaptic GluA1 significantly increased ($p < 0.001$; Figure 4A), consistent with generalized BDNF-LTP in previous reports (Caldeira et al., 2007; Ying et al., 2002). Surface GluA1 levels slightly decreased, but remained significantly high, during a follow-up incubation period in the presence of BDNF or without any drugs ($p < 0.05$; Figure 4A, right): a decaying component of surface GluA1 levels may be accounted for by an activity-dependent regulation of surface receptor degradation at active synapses. When BDNF-treated neurons were subsequently treated with TTX for 2 hr, surface GluA1 expression levels were markedly reduced to the levels observed prior to BDNF activation (Figure 4A; $p < 0.05$, BDNF → TTX versus "BDNF → BDNF" or "BDNF → no drug"; not significant, BDNF → TTX versus "No activation"). Because cell-wide Arc expression levels determined by western blot did not differ among these follow-up treatment groups (Figure S4A), the reduction in surface GluA1 levels at synapses may not directly correlate with global Arc expression per se but may reflect local synaptic Arc dynamics directly associated with local synaptic activity/inactivity. Strikingly, a clear

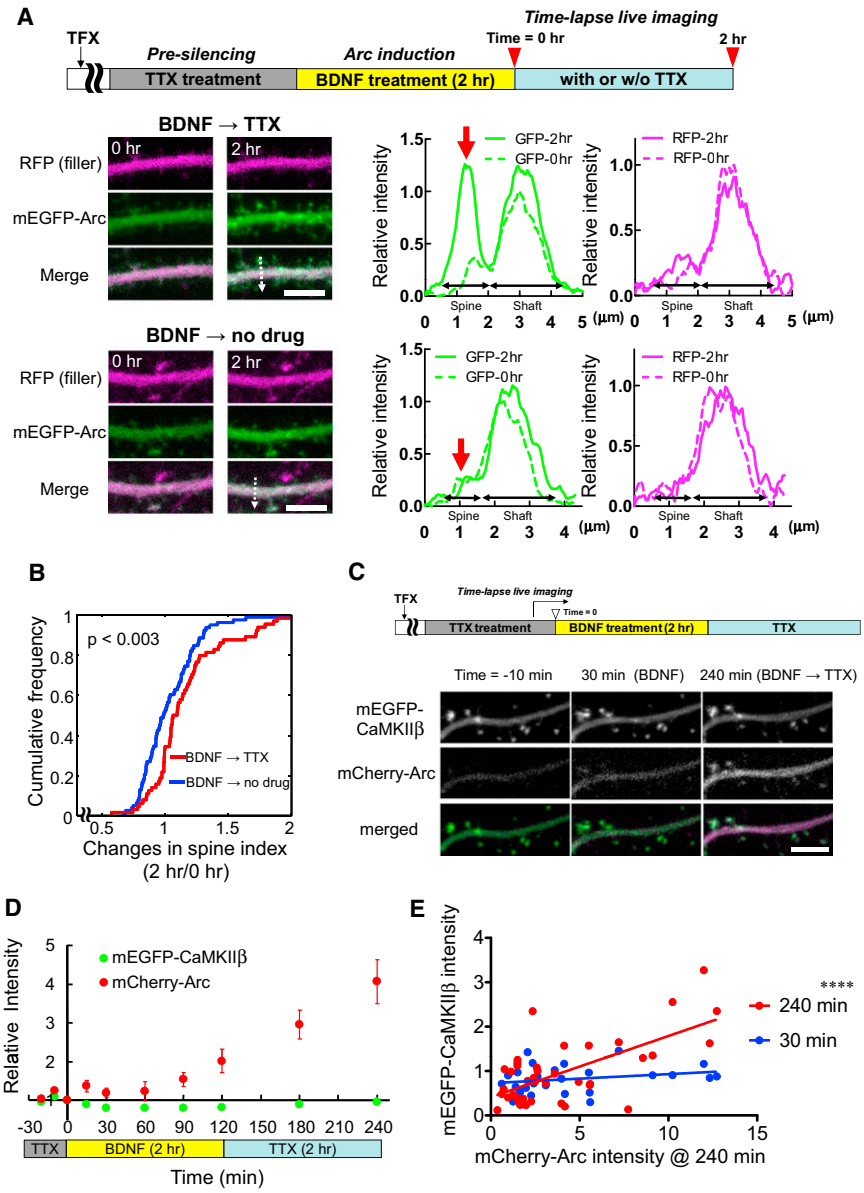

Figure 3. Inactivity-Induced Synaptic Accumulation of Arc in Living Neurons

(A and B) Live imaging of mEGFP-Arc accumulation in the spines during synaptic inactivity is shown. (A) Representative time-lapse images. Red arrows indicate the location of spines analyzed in the line profiles (dotted arrows in left panels). Scale bar, 5 μm. (B) A cumulative frequency histogram of spine index changes between 0 and 2 hr is illustrated (see Experimental Procedures).

(C–E) Time-lapse imaging of mEGFP-CaMKIIβ and activity-driven mCherry-Arc. (C) A schematic experimental diagram and representative time-lapse images are shown. Recording started before BDNF stimulation. Scale bar, 5 μm. (D) Time course of changes in averaged relative fluorescent intensities in spines. Error bars represent SEM. (E) Relationship between the intensity of mCherry-Arc at the end of imaging session (240 min) and those of mEGFP-CaMKIIβ at 30 and at 240 min, in individual spines is shown. ****p < 0.0001.

negative correlation was invariably detected at single synapses between the amounts of surface GluA1 and Arc IR that were coadjacent to the presynaptic marker vGlut1 (Figures 4B–4D). As a follow-up experiment of Figure 2C, we also measured surface GluA1 levels in spines that faced TeNT-expressing axons and compared them to those in adjacent nonsilenced spines (Figure S4B). The GluA1 levels were significantly lower in spines close to the TeNT axons than in neighboring control spines ($p < 0.05$), whereas control GFP expression had no effect (Figure S4C).

These results provide compelling evidence that the degree of maintenance of newly induced Arc protein in the synaptic pool quantitatively determines the turnover of GluA1 in an input-specific manner. Furthermore, the downregulation of GluA1 in Arc-containing synapses, but not in Arc-deficient synapses, is consistent with the idea that an inactivity-modulated concentration gradient of Arc plays a role in facilitating the clearance of initially upregulated GluA1 from weak synapses during the late phase of various forms of synaptic potentiation.

CaMKIIβ Acts as a Scaffold for Arc in Dendritic Spines

Because CaMKIIβ was enriched at dendritic spines (Figures 1A and 3C) and because we found evidence for the physical proximity and association between CaMKIIβ and Arc (Figures 1B, 1D, S1A, and S1C), we determined the effects of CaMKIIβ knockdown (using a small hairpin [sh] RNA vector) on Arc accumulation in the dendritic spines of neurons treated with BDNF followed by TTX (Figures 5A–5C). A line profile of fluorescence intensity from the tip of spine to the adjacent dendritic shaft revealed that Arc IR preferentially accumulated at the spines in mock-control cells (sh nega). In contrast, CaMKIIβ knockdown (sh β) effectively suppressed Arc accumulation in the spines (Figures 5A and 5C). This CaMKIIβ knockdown effect was not replicated by CaMKIIα knockdown (sh α) but could be rescued by coexpressing an RNAi-resistant WT CaMKIIβ (sh β + CaMKIIβ-WTres) (Figures 5B and 5C). Thus, the shRNA effect on Arc localization is genuinely mediated by a loss of CaMKIIβ (Figures 5C and S5A). The specificity and efficacy of the CaMKII knockdown using our shRNA vectors were confirmed by immunostaining (Figure S5B). Similar analyses on another PSD protein, Homer, showed that Homer accumulation in the spines was unaltered with either CaMKIIβ or CaMKIIα knockdown (Figures S5C and S5D), ruling out a general disruption of PSD organization by CaMKIIβ knockdown.

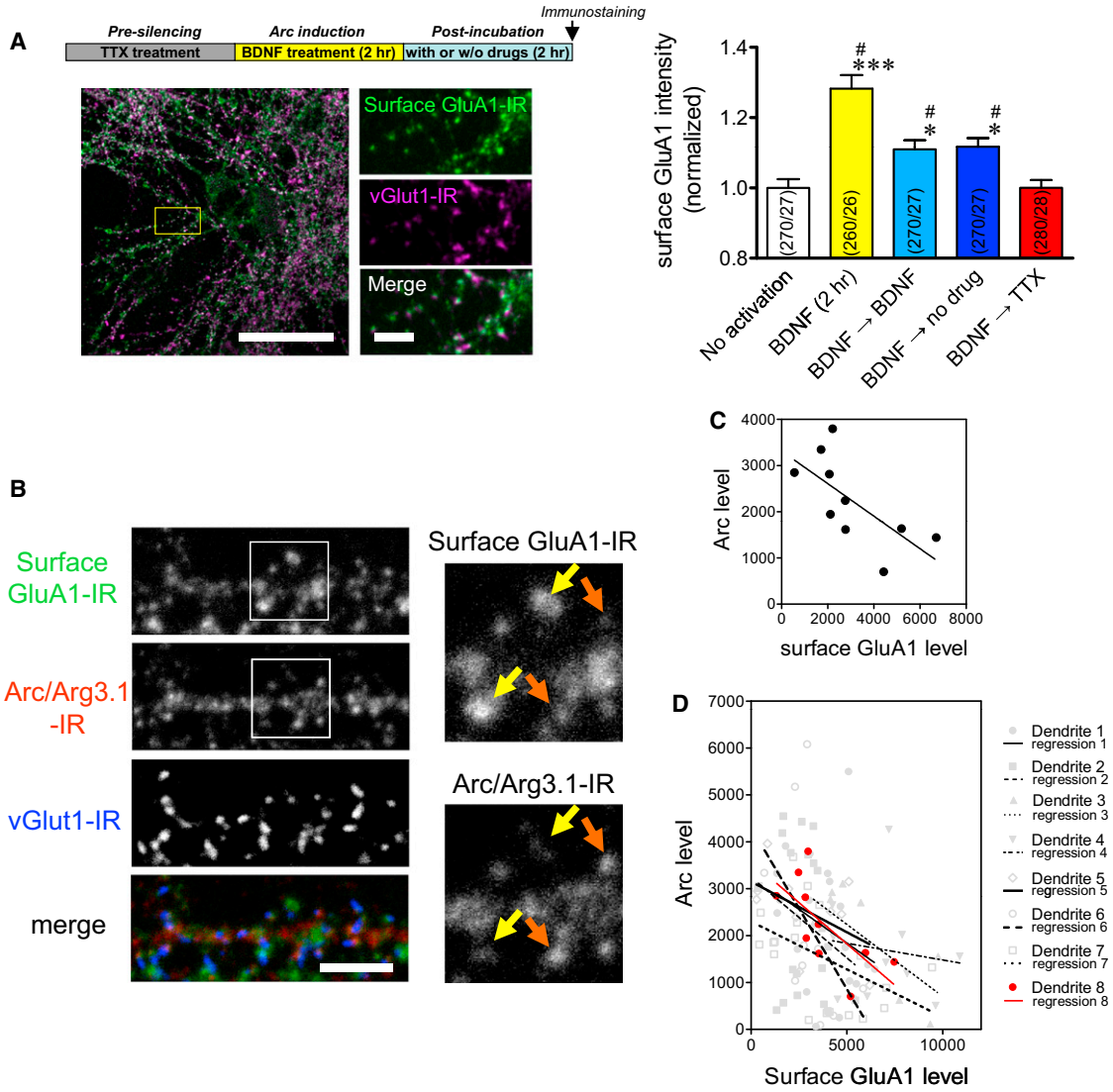

Figure 4. Synaptic Arc Content Is Inversely Correlated to Surface Expression Levels of GluA1 in Individual Synapses

(A) A period of inactivity that promotes synaptic Arc maintenance also results in reduced surface expression levels of GluA1. Left view is representative images of surface GluA1 IR juxtaposed to vGlut1 puncta in neurons treated with BDNF followed by TTX. A framed area (yellow box) in the left is expanded in the right. Neurons were first live stained for surface GluA1 (green) and then stained for vGlut1 (magenta) after fixation. Scale bars, 50 μm (left) and 5 μm (right). Right view shows quantification of the average intensity of GluA1 surface staining. Error bars represent SEM. *$p < 0.05$; ***$p < 0.001$ (compared to the no-activation control by ANOVA with a Tukey's test). #$p < 0.05$ (compared to "BDNF → TTX").

(B) Representative triple immunostaining of a dendritic segment from hippocampal neurons treated with BDNF followed by TTX is shown. Framed areas (white squares) in the left are expanded on the right. Some spines contained high-surface GluA1 signals but low Arc signals (yellow arrows), whereas others displayed the opposite pattern (orange arrows). Scale bar, 5 μm.

(C) Negative correlation of synaptic Arc and surface GluA1 levels at individual synapses is shown. The synaptic GulA1 and Arc levels in the dendritic segment shown in (B) were measured and plotted.

(D) Population data of the GluA1 and Arc expression analysis are shown. Lines represent the regression lines of individual dendritic segments from eight cells. Red symbols (Dendrite 8) and line are the same data shown in (C).

See also Figure S4.

We next performed a series of rescue experiments using several RNAi-resistant CaMKIIβ mutants (Figures 5D and S6A). Expression of a kinase-dead and autophosphorylation-deficient mutant K43M/T287Ares was as effective as WTres CaMKIIβ in rescuing the deficit in synaptic Arc accumulation caused by CaMKIIβ knockdown ($p < 0.01$). In contrast, a phospho-mimic, constitutively active mutant T287Dres was capable of rescuing to some extent, but not fully, the deficit in the synaptic Arc localization ($p < 0.05$ versus WT by K-S test, but also $p < 0.05$ versus the empty control by ANOVA with Tukey's test). In

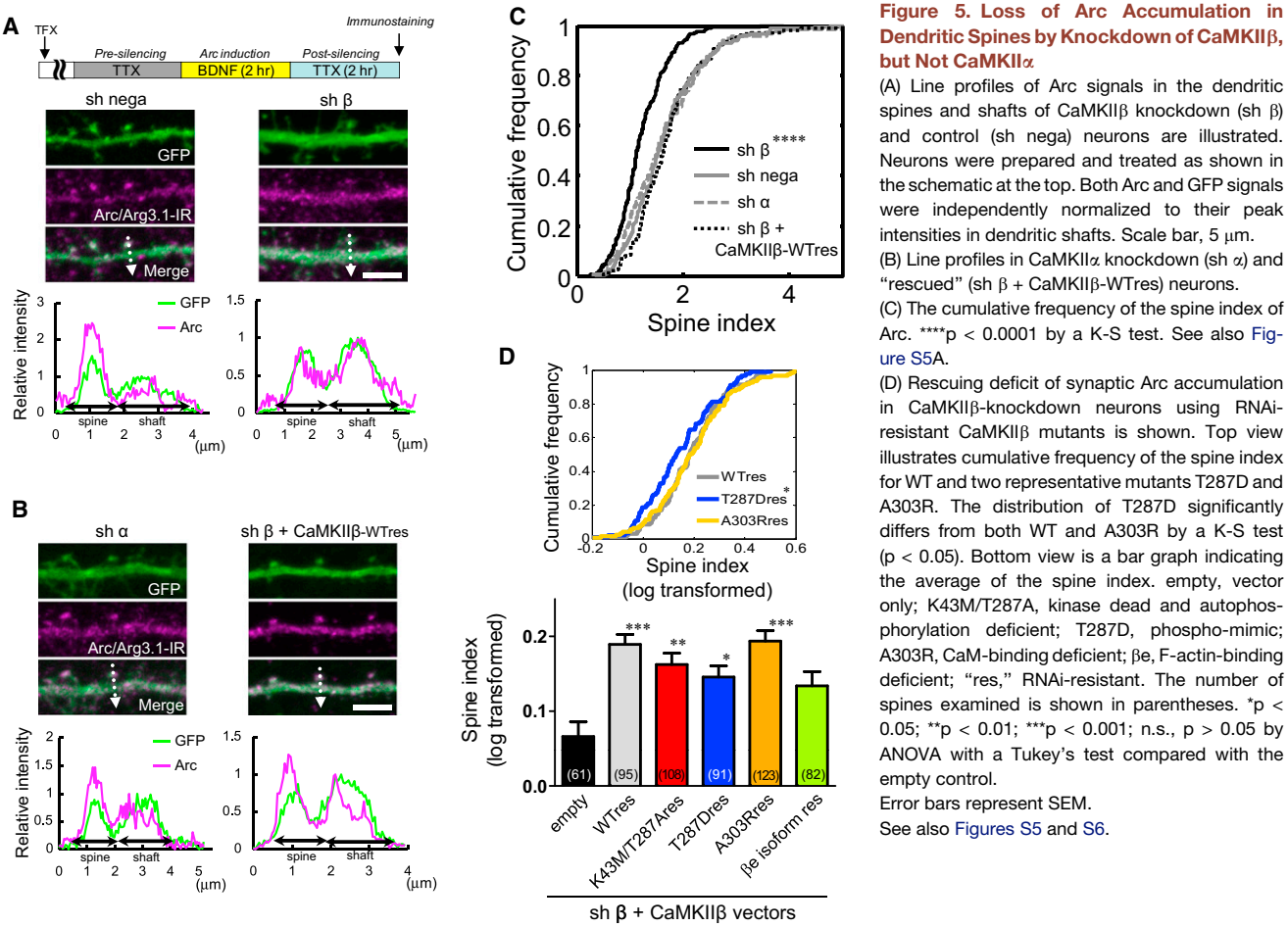

Figure 5. Loss of Arc Accumulation in Dendritic Spines by Knockdown of CaMKIIβ, but Not CaMKIIα

(A) Line profiles of Arc signals in the dendritic spines and shafts of CaMKIIβ knockdown (sh β) and control (sh nega) neurons are illustrated. Neurons were prepared and treated as shown in the schematic at the top. Both Arc and GFP signals were independently normalized to their peak intensities in dendritic shafts. Scale bar, 5 μm.

(B) Line profiles in CaMKIIα knockdown (sh α) and "rescued" (sh β + CaMKIIβ-WTres) neurons.

(C) The cumulative frequency of the spine index of Arc. ****$p < 0.0001$ by a K-S test. See also Figure S5A.

(D) Rescuing deficit of synaptic Arc accumulation in CaMKIIβ-knockdown neurons using RNAi-resistant CaMKIIβ mutants is shown. Top view illustrates cumulative frequency of the spine index for WT and two representative mutants T287D and A303R. The distribution of T287D significantly differs from both WT and A303R by a K-S test ($p < 0.05$). Bottom view is a bar graph indicating the average of the spine index. empty, vector only; K43M/T287A, kinase dead and autophosphorylation deficient; T287D, phospho-mimic; A303R, CaM-binding deficient; βe, F-actin-binding deficient; "res," RNAi-resistant. The number of spines examined is shown in parentheses. *$p < 0.05$; **$p < 0.01$; ***$p < 0.001$; n.s., $p > 0.05$ by ANOVA with a Tukey's test compared with the empty control.

Error bars represent SEM.

See also Figures S5 and S6.

keeping with these neuronal in situ results, in vitro GST-binding assays showed that a recombinant K43M/T287A (as well as a T287A) mutant protein showed strong Arc binding in the absence of Ca^{2+}/CaM to the same extent as a WT CaMKIIβ protein (Figures S6B and S6C), suggesting that the kinase activity per se does not contribute to Arc binding to CaMKIIβ. In contrast, a T287D mutant protein showed a much weakened, but residual, binding activity (Figure S6B). Because these results suggested the critical importance of the CaM-unbound closed conformation (Hudmon and Schulman, 2002) for Arc binding, we specifically tested this idea and found that expression of a constitutive CaM-binding-deficient mutant A303Rres was sufficient to restore synaptic Arc accumulation (Figure 5D). Interestingly, a recombinant protein of a non-F-actin binding CaMKIIβ isoform βe exhibited an in vitro Arc-binding activity similar to that of WT CaMKIIβ protein (Figure S6D), yet its expression only partially rescued the CaMKIIβ knockdown phenotype (Figure 5D). Overall, this is consistent with the idea that F-actin binding may be necessary for synaptic targeting of WT CaMKIIβ, but perhaps not directly for Arc accumulation per se. Taken together, these results strongly support the notion that activity-induced Arc is anchored at synapses through its interaction with a CaM-unbound CaMKIIβ during inactivity.

Increased Arc Maintenance in the Postsynapses after Cortical Activity Blockade In Vivo

We then asked whether the in vitro observations described above were relevant in vivo. To test this, we generated transgenic (Tg) mice in which mEGFP-Arc was driven by the *Arc* promoter (Figures S7A and S7B). We took advantage of the contralaterality of the mouse visual system to physiologically manipulate cortical activity/inactivity in a manner analogous to the aforementioned in vitro experiments, while keeping rigorous within-individual controls (Figures 6A and 6B). Following dark rearing, mice were exposed to light on both eyes for 4 hr to trigger strong bilateral activation of the primary visual cortex (V1); the neuronal activity of one V1 hemisphere was then shut off by injecting TTX into one eye, whereas the other eye was injected with PBS as a control (Figures 6A and 6B). Two control experiments were carried out. In the first control experiment, we confirmed that a similar intraocular TTX injection before light exposure effectively prevented V1 activation as shown by the lack of mEGFP-Arc induction after this procedure (Figure S7C). In the second control experiment, we tested whether the overall expression levels of the Arc protein reporter that was induced during the 4 hr light exposure were altered by a unilateral silencing due to monocular TTX injection, and we found that,

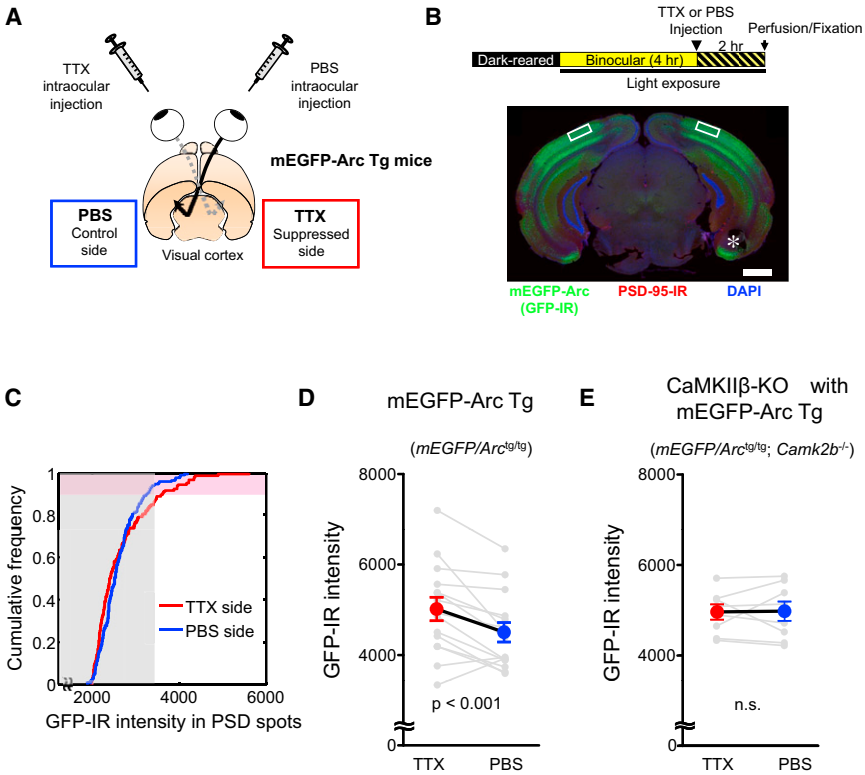

Figure 6. Enhancement of Arc Synaptic Accumulation with Inactivity and Its Dependency on CaMKIIβ In Vivo

(A) A schematic drawing of the intra-animal comparison of inactivated and control hemispheres is illustrated.

(B) A representative immunohistochemical section of mEGFP-Arc Tg mice underwent unilateral activity suppression after a 4 hr light exposure. A schematic paradigm is shown at the top. The layer 2/3 of the monocular zone of the primary visual cortex (boxed areas) was analyzed for quantification. Note that TTX injection after light exposure had little effect on the overall mEGFP-Arc expression. The asterisk (*) indicates the suppressed hemisphere. Scale bar, 1 mm.

(C) A representative intra-animal cumulative histogram comparison across hemispheres of mEGFP-Arc intensities in PSD spots is illustrated. Because most mEGFP-Arc signals were below background levels (gray shaded area), the average of the top 10% intensities (pink shaded area) was used for the population analysis in (D).

(D) Population analysis of the intra-animal comparisons is shown. The mEGFP-Arc intensities at the TTX-affected side were significantly higher than those of the control side ($p < 0.001$, paired-t test) (n = 15 animals).

(E) The effect of CaMKIIβ null genotype on Arc synaptic localization in vivo is illustrated. The enhancement of mEGFP-Arc intensities in the TTX-affected side was abolished in this genotype (n = 8 animals). n.s., not significant.

Error bars represent SEM.

See also Figure S7.

similar to our in vitro observations, the overall degree of mEGFP-Arc induction did not differ between the two hemispheres (Figure 6B). Having ascertained these controls, we then blindly quantified the expression levels of synaptic mEGFP-Arc in both hemispheres by measuring GFP IR in PSD-95-positive PSDs with high-power microscopy (Figure S7D) and compared the intensity distributions between the experimental and control hemispheres (Figures 6C and 6D). The synaptic mEGFP-Arc signals were found to be significantly higher in the hemisphere that was contralateral to the TTX-treated eye as opposed to the control ipsilateral one ($p < 0.001$, paired t test) (Figure 6D). No such difference was detected for the levels of PSD-95 IR (Figure S7E).

We further assessed the inactivity-dependent regulation of synaptic Arc levels in a CaMKIIβ null genotype in vivo, with the same experimental paradigm, using a cross of the CaMKIIβ-KO and the mEGFP-Arc reporter Tg mouse line. Blind analysis showed no difference in mEGFP-Arc levels in the PSD in the V1 between the silenced and control hemispheres, in the mEGFP-Arc Tg/CaMKIIβ null-combined genotype (Figure 6E). The distribution of PSD-95 IR was not significantly altered between hemispheres, either in the WT or in the CaMKIIβ-KO (Figures S7E and S7F), in keeping with a prior anatomical observation in CaMKIIβ null mice that reported little change in synaptic morphology (Borgesius et al., 2011).

Taken together, these in vivo results provide strong evidence that activity-induced Arc protein is preferentially targeted to inactive CaMKIIβ at weak synapses as a consequence of the sequential history of synaptic activity and inactivity in the brain.

Preferential Arc Targeting into Weak Synapses following Plasticity-Inducing Stimulation

Our data suggested that Arc protein is anchored in less-active synapses through its interaction with an inactive form of CaMKIIβ. Is activity-induced Arc then directed less to potentiated synapses and more to nonpotentiated synapses following plasticity-inducing stimulation? We tested this notion in cultured neurons expressing a volume marker RFP and activity-regulated mEGFP-Arc. We applied high-frequency electrical field stimulation that evoked stimulus-induced volume expansion in a large population of spines (Figure 7A). Following stimulation, the emerging fluorescence from newly synthesized mEGFP-Arc could be coimaged in a sizable proportion of synapses along with volume expansion, a reliable index of synaptic potentiation (Matsuzaki et al., 2004) (Figure 7C; see also Movie S1). When spines were classified into "expanded" and "non-expanded" groups (see Experimental Procedures), the expanded group showed robust and long-lasting increases (>3 hr), whereas the volume of the nonexpanded group remained stable (Figure 7C). Analysis of the volume-corrected mEGFP-Arc level in single spines raised the possibility that high levels of mEGFP-Arc were found in nonexpanded, rather than expanded, spines at 3 hr after the stimulation (Figure 7B). Indeed, the mEGFP-Arc

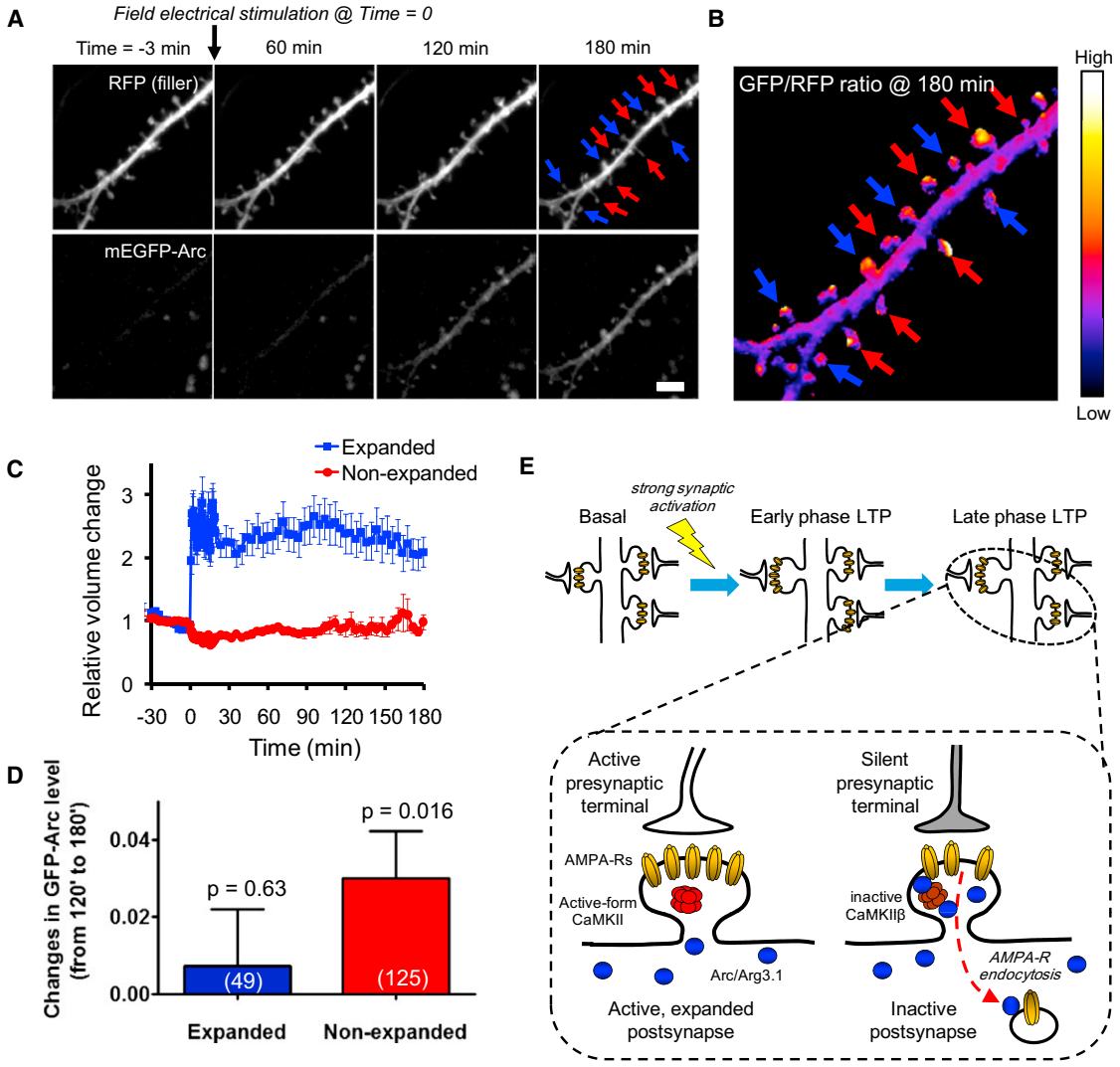

Figure 7. Activity-Induced Arc Accumulates at Nonexpanded Synapses Rather Than Expanded Synapses following Structural Plasticity-Inducing Stimulation

(A) Time-lapse images of activity-induced mEGFP-Arc and a volume marker TagRFP following high-frequency field electrical stimulation that induces spine volume expansion are shown. Expanded (blue arrows) and nonexpanded (red arrows) spines are illustrated for clarity. Scale bar, 5 μm. See also Movie S1.

(B) A pseudo-color GFP/RFP ratio map of the dendritic segment shown in (A) at 180 min after the stimulation is illustrated.

(C) In expanded spines, high-frequency electrical stimulation induced long-lasting volume expansion that lasted for at least 3 hr after the stimulation, whereas no apparent changes were observed in nonexpanded spines.

(D) The GFP-Arc levels (shown as the ratio at 180 and 120 min, and log transformed), in nonexpanded spines, significantly increased during 120–180 min after the stimulation ($p = 0.016$), but not in expanded spines ($p = 0.63$). Error bars represent SEM.

(E) Arc action on AMPA-R clearance at active and inactive synapses is illustrated. After synaptic potentiation, the surface AMPA-Rs are augmented at the synapses that receive strong inputs, whereas a cell-wide Arc induction is also triggered. During the late phase of potentiation, Arc is differently maintained in the synapses depending on the amount and history of synaptic activity. In the synapses that receive frequent inputs (active or late LTP-like synapses), CaMKIIβ is more likely to be activated, and thus, its interaction with Arc is largely weakened. As a result, Arc may diffuse out from the synapses more freely. In contrast, synapses with low activity (inactive or early LTP-like synapses) are more likely to contain an inactive form of CaMKIIβ, which provides a scaffold for Arc at the synapse. The CaMKIIβ-stabilized Arc may efficiently contribute to promoting AMPA-R clearance from the inactive synapse. Through such an inactivity-dependent control of synaptic dynamics, Arc may contribute to synaptic homeostasis and restrict the resident time of newly recruited surface AMPA-Rs at inactive synapses, whereas active, potentiated synapses remain unaffected.

levels significantly increased between 2 and 3 hr after the onset of the stimulation in the nonexpanded group ($p = 0.016$), but not in the expanded group (Figure 7D).

Taken together, our data are consistent with an inverse synaptic-tagging role of activity-induced Arc, in which Arc is preferentially targeted to less-active synapses than to expanded

potentiated synapses during the late phase of synaptic potentiation (Figure 7E).

DISCUSSION

Clearance of Upregulated GluA1 in Inactive Synapses via Local Inactivity-Controlled Enrichment of Arc through Dynamic Interaction with CaMKIIβ

Here, we demonstrated that the level of local synaptic *in*activity critically determines the kinetics of activity-induced Arc turnover at the synapse. We further discovered that this mechanism is made possible by a heightened affinity between an inactive form of CaMKIIβ and Arc at synapses, which allows Arc to be preferentially maintained at inactive synapses rather than active synapses. Arc targeting to less-active synapses via CaMKIIβ thus provides a tunable mechanism for synapse-specific control of AMPA-R trafficking according to the history of local synaptic activity and inactivity.

Our results demonstrate that an inactive form of CaMKIIβ, rather than CaMKIIα, has a more dominant role in Arc regulation at synapses in neurons, both in vitro and in vivo, especially under synaptically silenced conditions following Arc induction. We cannot, however, rule out a possible role for CaMKIIα in Arc regulation under other conditions (Donai et al., 2003).

Previously, CaMKIIβ, together with CaMKIIα, was shown to translocate into the spines from the dendritic shaft upon strong synaptic inputs (Shen and Meyer, 1998). Our finding that Arc preferentially binds to inactive CaMKIIβ suggests that the α/β ratio in a heteromeric CaMKII complex may play a determinant role in enabling the CaMKII complex to retain Arc in the spines. Although it remains to be shown how the history of the spine's activity exactly specifies the composition of the CaMKII complex, a role for local translation of CaMKIIα has previously been proposed by Miller et al. (2002). Overall, at the single-spine level, the dynamics of the synaptic CaMKII complex might provide the basis for assigning the late outcome of plasticity, perhaps as a function of an enhanced CaMKIIα protein synthesis (in strongly stimulated [late LTP-like] spines) or via a privileged CaMKIIβ-Arc interaction (in weakly stimulated [early LTP-like] spines). Because the majority of inactive CaMKIIβ reside in the dendritic shaft, further studies are needed to elucidate key mechanisms that allow Arc to preferentially interact with a specific pool of inactive CaMKIIβ that resides within the spines.

Structurally, CaMKIIβ has a unique F-actin-binding insertion between the regulatory and association domains (O'Leary et al., 2006; Okamoto et al., 2007; Shen and Meyer, 1998). We found that the same condition that favors an F-actin-CaMKIIβ complex formation, namely the absence of Ca^{2+}/CaM (O'Leary et al., 2006; Okamoto et al., 2007), also promotes Arc interaction with an inactive CaMKIIβ (Figure 1). However, an F-actin-binding insertion in CaMKIIβ was dispensable for Arc binding (Figure S6). These observations imply that, whereas a sustained level of low Ca^{2+} concentration during synaptic inactivity would be consistent with the costabilization of both F-actin-CaMKIIβ and Arc-CaMKIIβ complexes within the synapses, the two complexes may be separable.

Capturing of Arc by CaMKIIβ as an Inverse Synaptic-Tagging Process that Operates at Inactive Synapses during Late-Phase Plasticity

The synaptic tagging and capture theory has recently provided an attractive framework that accounts for the persistence in the late phase of long-term, synapse-specific, macromolecule synthesis-dependent forms of neuronal plasticity (Frey and Morris, 1997; Redondo et al., 2010). Although several candidate molecules and signaling pathways have been proposed as synaptic tags or active synapse-targeted plasticity-related proteins (PRPs), the relevant combination of synaptic tags in the potentiated spines and of the captured PRPs, to date, remains largely unknown (Navakkode et al., 2004; Okada et al., 2009; Redondo et al., 2010). Our results indicate an alternative, nonmutually exclusive, possibility. In this scenario, "inverse tags" may be specifically generated to sort newly synthesized PRPs to inactive synapses through an *in*activity-sensing mechanism. The selective avoidance of actively tagged synapses by a negative plasticity factor, such as Arc, via a preferential interaction with an "inverse tag," such as an inactive CaMKIIβ, may thus be considered the conceptual opposite of the classical notion of synaptic tagging, or an "inverse synaptic tagging" process. Preventing undesired synaptic enhancement at weak synapses, while sparing potentiated synapses, will ensure that the contrast between strong and weak inputs remains stable over time (Figure 7E).

Previous studies have established that activity-induced *Arc* mRNA and protein are enriched in dendritic regions in the DG that receive layer-specific, high-frequency stimulation (Steward et al., 1998; Moga et al., 2004). It has thus been widely assumed, though not directly tested, that Arc may be targeted to potentiated/stimulated synapses. Our results suggest that the actual sites of the Arc accumulation in previous studies might have been inactive synapses and/or dendritic shafts within the activated areas. The role of Arc at less-active synapses may readily reconcile apparently contradictory roles of Arc during the late phase of various forms of long-term synaptic plasticity and during homeostatic plasticity and synaptic scaling (Chowdhury et al., 2006; Rial Verde et al., 2006; Shepherd et al., 2006). Our findings are also in keeping with an activity-dependent degradation of Arc through Ube3a, which may also contribute to the exclusion of Arc in active synapses (Greer et al., 2010).

The presence of such dual mechanisms for Arc regulation would be an effective way to achieve late-phase consolidation of the synaptic weight differences between active and inactive synapses following a strong synaptic potentiation (Figure 7E), such as during late-phase LTP or sharpening of sensory-evoked response tuning in the neocortex (McCurry et al., 2010; Wang et al., 2006). Our findings pave the way for elucidating the role of the signaling from the nucleus to synapses at unprecedented resolution and help advance our understanding of the information-processing role of activity-dependent genes at single synapses.

EXPERIMENTAL PROCEDURES

Plasmids and Antibodies

Detailed information regarding plasmids and antibodies used in this work is described in the Extended Experimental Procedures.

Animals

Sprague-Dawley rats were used for neuronal culture preparation. A line of Tg mice harboring the Arc-promoter mEGFP-Arc was generated by microinjection of a mEGFP-Arc cDNA construct into fertilized C57BL/6 mouse eggs. Gene targeting of CaMKIIβ was carried out in the C57BL/6-derived embryonic stem cell line RENKA (Mishina and Sakimura, 2007) by homologous recombination. Detailed characterization of CaMKIIβ null mice will be described elsewhere (K. Sakimura and K.A., unpublished data).

All animal experiments were carried out in accordance with the regulations and guidelines for the care and use of experimental animals at the University of Tokyo and Niigata University and were approved by the institutional review committees of the University of Tokyo Graduate School of Medicine and Niigata University Brain Research Institute.

Primary Neuronal Cultures

Hippocampal neurons were prepared from the CA1/CA3 regions of the hippocampus of 1-day-old (P1) Sprague-Dawley rats as described elsewhere by Bito et al. (1996) and Kawashima et al. (2009). At 14–24 days in vitro (DIV), the cells were incubated in a growth medium containing TTX (2 μM; Wako, Osaka, Japan) for 24 hr. The neurons were then treated with BDNF (50 ng/ml, generously provided by Dainippon Sumitomo Pharma, Osaka, Japan) for 2 hr, further treated with a medium containing channel blockers or inhibitors, and then fixed for immunostaining.

Purification of Recombinant Proteins and In Vitro Binding

Bacterially expressed recombinant GST-Arc was purified with glutathione-Sepharose 4B beads (GE Healthcare). Recombinant CaMKII and its mutant proteins were expressed in HEK293T cells and purified with CaM-Sepharose 4B beads (GE Healthcare). Detailed protocols for in vitro-binding assays are provided in the Extended Experimental Procedures.

Image Acquisition and Analyses of Immunostained Neurons

All image acquisition and analyses were performed in a blind manner. Confocal z stack fluorescence images were obtained using a LSM510 confocal laser microscopy system (Carl Zeiss). All stacked images were projected into single planes by summation and used for quantitative analyses as described below.

For the evaluation of Arc localization in the PSD, PSD spots were defined on the basis of PSD-95 IR clustering essentially as described previously by Nonaka et al. (2006). All PSD-95 spots that were well separated from the dendritic shaft of an Arc-IR-positive dendrite were analyzed, and a corresponding non-PSD area that was adjacent to a given PSD spot was defined within dendritic shafts for each PSD spot. After background subtraction, the average intensity of Arc immunofluorescence was measured. The intensity ratio of PSD to non-PSD was designated as the Arc accumulation index.

For RNAi and rescue experiments, dendritic segments of GFP (a marker of the shRNA vectors) and Arc double-positive neurons were imaged. Dendritic spine accumulation was evaluated by analyzing the fluorescence-intensity profiles at spine and shaft in dendrites.

Detailed procedures are provided in the Extended Experimental Procedures.

Live Imaging and Data Analysis

Hippocampal neurons plated on glass-bottom dishes (MatTek) were cotransfected with the pGL4.11-Arc7000-mEGFP-Arc-UTRs and a marker plasmid pTagRFP-C (Evrogen), at 7–9 DIV. Series of z stack images for both GFP and RFP signals were acquired at 16–22 DIV. The z stack images were projected into a single-plane image by summation, and the fluorescence line profiles of spines and adjacent dendritic shafts were measured. An index for spine accumulation was defined as follows:

$$\text{Spine index} = \frac{(\text{GFP}_{\text{spine}}/\text{GFP}_{\text{shaft}})}{(\text{RFP}_{\text{spine}}/\text{RFP}_{\text{shaft}})},$$

where $\text{GFP}_{\text{spine}}$ and $\text{GFP}_{\text{shaft}}$ represent the peak green fluorescent intensities, whereas $\text{RFP}_{\text{spine}}$ and $\text{RFP}_{\text{shaft}}$ indicate the peak red fluorescent intensities in the spine and the shaft, respectively. The ratios of spine indices before and 2 hr after follow-up incubation of individual spine-shaft pairs were calculated for a cumulative frequency presentation. Arc/CaMKII dual imaging was done in neurons transfected with pGL4.11-Arc7000-mCherry-Arc-UTRs and pcDNA3-mEGFP-CaMKIIβ. Detailed procedures are provided in the Extended Experimental Procedures.

Surface AMPA-R Labeling

Extracellular AMPA-Rs were labeled in live hippocampal neurons (17–18 DIV) using an anti-GluA1 antibody (Alomone Labs), essentially as described previously by Chowdhury et al. (2006) and Shepherd et al. (2006). The quantification of surface GluA1 puncta was carried out using a custom-made macro running on MetaMorph software (Universal Imaging). All image analyses were performed by a person who was blinded to the experimental conditions. Detailed procedures are provided in the Extended Experimental Procedures.

Statistical Analysis

Statistical analyses were performed using Prism 5.0 (GraphPad Software), Excel (Microsoft), MATLAB (MathWorks), or JMP 8 (SAS Institute). Log transformation was applied to correct possible skewness of data distribution where appropriate. All data are expressed as the mean ± SEM, unless indicated otherwise.

SUPPLEMENTAL INFORMATION

Supplemental Information includes Extended Experimental Procedures, seven figures, and one movie and can be found with this article online at doi:10.1016/j.cell.2012.02.062.

ACKNOWLEDGMENTS

We thank H. Schulman and T. Meyer for several CaMKII constructs, R.Y. Tsien for mCherry cDNA, A. Miyawaki for Venus cDNA, M. Yamamoto for GFP-TeNT cDNA, K.U. Bayer for pmEGFP-CaMKIIβe cDNA, and M. Watanabe for an anti-vGlut1 antibody, and all members of the Bito laboratory for support. BDNF was provided by Dainippon Sumitomo Pharma, Osaka, Japan. We thank T. Bonhoeffer, K. Deisseroth, R.G.M. Morris, V. Naegerl, R. Redondo, M. van Rossum, M. Schnitzer, and R.W. Tsien for valuable comments on an earlier version of this work, and R. Huganir for critical reading of the manuscript. We are indebted to Y. Kondo, K. Saiki, A. Adachi-Morishima, R. Gyobu, and T. Kinbara for assistance. This work was supported in part by Grants-in-Aid (WAKATE, KIBAN, START, CBSN) from JSPS and MEXT of Japan (to H.O., M.N., S.T-K., K. Sakimura, and H.B.), from the MHLW of Japan (to H.O. and H.B.), by a grant from NIMH (to P.F.W.), and by awards from the HFSP (to H.O. and H.B.) and from the Shimadzu Foundation, Kowa Life Science Foundation, Takeda Science Foundation, and the Mitsubishi Foundation (to H.B.). Y.I., N.Y-K., K. Suzuki, and T.K. are JSPS predoctoral fellows.

Received: March 30, 2011
Revised: November 9, 2011
Accepted: February 21, 2012
Published: May 10, 2012

REFERENCES

Béïque, J.C., Na, Y., Kuhl, D., Worley, P.F., and Huganir, R.L. (2011). Arc-dependent synapse-specific homeostatic plasticity. Proc. Natl. Acad. Sci. USA *108*, 816–821.

Bito, H., Deisseroth, K., and Tsien, R.W. (1996). CREB phosphorylation and dephosphorylation: a $Ca^{(2+)}$- and stimulus duration-dependent switch for hippocampal gene expression. Cell *87*, 1203–1214.

Borgesius, N.Z., van Woerden, G.M., Buitendijk, G.H., Keijzer, N., Jaarsma, D., Hoogenraad, C.C., and Elgersma, Y. (2011). βCaMKII plays a nonenzymatic role in hippocampal synaptic plasticity and learning by targeting αCaMKII to synapses. J. Neurosci. *31*, 10141–10148.

Caldeira, M.V., Melo, C.V., Pereira, D.B., Carvalho, R., Correia, S.S., Backos, D.S., Carvalho, A.L., Esteban, J.A., and Duarte, C.B. (2007). Brain-derived neurotrophic factor regulates the expression and synaptic delivery of alpha-amino-3-hydroxy-5-methyl-4-isoxazole propionic acid receptor subunits in hippocampal neurons. J. Biol. Chem. *282*, 12619–12628.

Chowdhury, S., Shepherd, J.D., Okuno, H., Lyford, G., Petralia, R.S., Plath, N., Kuhl, D., Huganir, R.L., and Worley, P.F. (2006). Arc/Arg3.1 interacts with the endocytic machinery to regulate AMPA receptor trafficking. Neuron *52*, 445–459.

Donai, H., Sugiura, H., Ara, D., Yoshimura, Y., Yamagata, K., and Yamauchi, T. (2003). Interaction of Arc with CaM kinase II and stimulation of neurite extension by Arc in neuroblastoma cells expressing CaM kinase II. Neurosci. Res. *47*, 399–408.

Flavell, S.W., Cowan, C.W., Kim, T.K., Greer, P.L., Lin, Y., Paradis, S., Griffith, E.C., Hu, L.S., Chen, C., and Greenberg, M.E. (2006). Activity-dependent regulation of MEF2 transcription factors suppresses excitatory synapse number. Science *311*, 1008–1012.

Frey, U., and Morris, R.G. (1997). Synaptic tagging and long-term potentiation. Nature *385*, 533–536.

Greer, P.L., Hanayama, R., Bloodgood, B.L., Mardinly, A.R., Lipton, D.M., Flavell, S.W., Kim, T.K., Griffith, E.C., Waldon, Z., Maehr, R., et al. (2010). The Angelman Syndrome protein Ube3A regulates synapse development by ubiquitinating arc. Cell *140*, 704–716.

Guzowski, J.F., McNaughton, B.L., Barnes, C.A., and Worley, P.F. (1999). Environment-specific expression of the immediate-early gene Arc in hippocampal neuronal ensembles. Nat. Neurosci. *2*, 1120–1124.

Guzowski, J.F., Lyford, G.L., Stevenson, G.D., Houston, F.P., McGaugh, J.L., Worley, P.F., and Barnes, C.A. (2000). Inhibition of activity-dependent arc protein expression in the rat hippocampus impairs the maintenance of long-term potentiation and the consolidation of long-term memory. J. Neurosci. *20*, 3993–4001.

Hudmon, A., and Schulman, H. (2002). Neuronal CA2+/calmodulin-dependent protein kinase II: the role of structure and autoregulation in cellular function. Annu. Rev. Biochem. *71*, 473–510.

Kawashima, T., Okuno, H., Nonaka, M., Adachi-Morishima, A., Kyo, N., Okamura, M., Takemoto-Kimura, S., Worley, P.F., and Bito, H. (2009). Synaptic activity-responsive element in the Arc/Arg3.1 promoter essential for synapse-to-nucleus signaling in activated neurons. Proc. Natl. Acad. Sci. USA *106*, 316–321.

Link, W., Konietzko, U., Kauselmann, G., Krug, M., Schwanke, B., Frey, U., and Kuhl, D. (1995). Somatodendritic expression of an immediate early gene is regulated by synaptic activity. Proc. Natl. Acad. Sci. USA *92*, 5734–5738.

Lyford, G.L., Yamagata, K., Kaufmann, W.E., Barnes, C.A., Sanders, L.K., Copeland, N.G., Gilbert, D.J., Jenkins, N.A., Lanahan, A.A., and Worley, P.F. (1995). Arc, a growth factor and activity-regulated gene, encodes a novel cytoskeleton-associated protein that is enriched in neuronal dendrites. Neuron *14*, 433–445.

Matsuzaki, M., Honkura, N., Ellis-Davies, G.C., and Kasai, H. (2004). Structural basis of long-term potentiation in single dendritic spines. Nature *429*, 761–766.

McCurry, C.L., Shepherd, J.D., Tropea, D., Wang, K.H., Bear, M.F., and Sur, M. (2010). Loss of Arc renders the visual cortex impervious to the effects of sensory experience or deprivation. Nat. Neurosci. *13*, 450–457.

Messaoudi, E., Kanhema, T., Soulé, J., Tiron, A., Dagyte, G., da Silva, B., and Bramham, C.R. (2007). Sustained Arc/Arg3.1 synthesis controls long-term potentiation consolidation through regulation of local actin polymerization in the dentate gyrus in vivo. J. Neurosci. *27*, 10445–10455.

Miller, S., Yasuda, M., Coats, J.K., Jones, Y., Martone, M.E., and Mayford, M. (2002). Disruption of dendritic translation of CaMKIIalpha impairs stabilization of synaptic plasticity and memory consolidation. Neuron *36*, 507–519.

Mishina, M., and Sakimura, K. (2007). Conditional gene targeting on the pure C57BL/6 genetic background. Neurosci. Res. *58*, 105–112.

Moga, D.E., Calhoun, M.E., Chowdhury, A., Worley, P., Morrison, J.H., and Shapiro, M.L. (2004). Activity-regulated cytoskeletal-associated protein is localized to recently activated excitatory synapses. Neuroscience *125*, 7–11.

Navakkode, S., Sajikumar, S., and Frey, J.U. (2004). The type IV-specific phosphodiesterase inhibitor rolipram and its effect on hippocampal long-term potentiation and synaptic tagging. J. Neurosci. *24*, 7740–7744.

Nedivi, E., Hevroni, D., Naot, D., Israeli, D., and Citri, Y. (1993). Numerous candidate plasticity-related genes revealed by differential cDNA cloning. Nature *363*, 718–722.

Nonaka, M., Doi, T., Fujiyoshi, Y., Takemoto-Kimura, S., and Bito, H. (2006). Essential contribution of the ligand-binding beta B/beta C loop of PDZ1 and PDZ2 in the regulation of postsynaptic clustering, scaffolding, and localization of postsynaptic density-95. J. Neurosci. *26*, 763–774.

Okada, D., Ozawa, F., and Inokuchi, K. (2009). Input-specific spine entry of soma-derived Vesl-1S protein conforms to synaptic tagging. Science *324*, 904–909.

Okamoto, K., Narayanan, R., Lee, S.H., Murata, K., and Hayashi, Y. (2007). The role of CaMKII as an F-actin-bundling protein crucial for maintenance of dendritic spine structure. Proc. Natl. Acad. Sci. USA *104*, 6418–6423.

O'Leary, H., Lasda, E., and Bayer, K.U. (2006). CaMKIIbeta association with the actin cytoskeleton is regulated by alternative splicing. Mol. Biol. Cell *17*, 4656–4665.

Park, S., Park, J.M., Kim, S., Kim, J.A., Shepherd, J.D., Smith-Hicks, C.L., Chowdhury, S., Kaufmann, W., Kuhl, D., Ryazanov, A.G., et al. (2008). Elongation factor 2 and fragile X mental retardation protein control the dynamic translation of Arc/Arg3.1 essential for mGluR-LTD. Neuron *59*, 70–83.

Peebles, C.L., Yoo, J., Thwin, M.T., Palop, J.J., Noebels, J.L., and Finkbeiner, S. (2010). Arc regulates spine morphology and maintains network stability in vivo. Proc. Natl. Acad. Sci. USA *107*, 18173–18178.

Plath, N., Ohana, O., Dammermann, B., Errington, M.L., Schmitz, D., Gross, C., Mao, X., Engelsberg, A., Mahlke, C., Welzl, H., et al. (2006). Arc/Arg3.1 is essential for the consolidation of synaptic plasticity and memories. Neuron *52*, 437–444.

Ploski, J.E., Pierre, V.J., Smucny, J., Park, K., Monsey, M.S., Overeem, K.A., and Schafe, G.E. (2008). The activity-regulated cytoskeletal-associated protein (Arc/Arg3.1) is required for memory consolidation of pavlovian fear conditioning in the lateral amygdala. J. Neurosci. *28*, 12383–12395.

Qian, Z., Gilbert, M.E., Colicos, M.A., Kandel, E.R., and Kuhl, D. (1993). Tissue-plasminogen activator is induced as an immediate-early gene during seizure, kindling and long-term potentiation. Nature *361*, 453–457.

Ramírez-Amaya, V., Vazdarjanova, A., Mikhael, D., Rosi, S., Worley, P.F., and Barnes, C.A. (2005). Spatial exploration-induced Arc mRNA and protein expression: evidence for selective, network-specific reactivation. J. Neurosci. *25*, 1761–1768.

Redondo, R.L., Okuno, H., Spooner, P.A., Frenguelli, B.G., Bito, H., and Morris, R.G. (2010). Synaptic tagging and capture: differential role of distinct calcium/calmodulin kinases in protein synthesis-dependent long-term potentiation. J. Neurosci. *30*, 4981–4989.

Rial Verde, E.M., Lee-Osbourne, J., Worley, P.F., Malinow, R., and Cline, H.T. (2006). Increased expression of the immediate-early gene arc/arg3.1 reduces AMPA receptor-mediated synaptic transmission. Neuron *52*, 461–474.

Shen, K., and Meyer, T. (1998). In vivo and in vitro characterization of the sequence requirement for oligomer formation of Ca2+/calmodulin-dependent protein kinase IIalpha. J. Neurochem. *70*, 96–104.

Shepherd, J.D., Rumbaugh, G., Wu, J., Chowdhury, S., Plath, N., Kuhl, D., Huganir, R.L., and Worley, P.F. (2006). Arc/Arg3.1 mediates homeostatic synaptic scaling of AMPA receptors. Neuron *52*, 475–484.

Smith-Hicks, C., Xiao, B., Deng, R., Ji, Y., Zhao, X., Shepherd, J.D., Posern, G., Kuhl, D., Huganir, R.L., Ginty, D.D., et al. (2010). SRF binding to SRE 6.9 in the Arc promoter is essential for LTD in cultured Purkinje cells. Nat. Neurosci. *13*, 1082–1089.

Steward, O., Wallace, C.S., Lyford, G.L., and Worley, P.F. (1998). Synaptic activation causes the mRNA for the IEG Arc to localize selectively near activated postsynaptic sites on dendrites. Neuron *21*, 741–751.

Wang, K.H., Majewska, A., Schummers, J., Farley, B., Hu, C., Sur, M., and Tonegawa, S. (2006). In vivo two-photon imaging reveals a role of arc in enhancing orientation specificity in visual cortex. Cell *126*, 389–402.

Waung, M.W., Pfeiffer, B.E., Nosyreva, E.D., Ronesi, J.A., and Huber, K.M. (2008). Rapid translation of Arc/Arg3.1 selectively mediates mGluR-dependent LTD through persistent increases in AMPAR endocytosis rate. Neuron *59*, 84–97.

Worley, P.F., Bhat, R.V., Baraban, J.M., Erickson, C.A., McNaughton, B.L., and Barnes, C.A. (1993). Thresholds for synaptic activation of transcription factors in hippocampus: correlation with long-term enhancement. J. Neurosci. *13*, 4776–4786.

Yamamoto, M., Wada, N., Kitabatake, Y., Watanabe, D., Anzai, M., Yokoyama, M., Teranishi, Y., and Nakanishi, S. (2003). Reversible suppression of glutamatergic neurotransmission of cerebellar granule cells in vivo by genetically manipulated expression of tetanus neurotoxin light chain. J. Neurosci. *23*, 6759–6767.

Ying, S.W., Futter, M., Rosenblum, K., Webber, M.J., Hunt, S.P., Bliss, T.V., and Bramham, C.R. (2002). Brain-derived neurotrophic factor induces long-term potentiation in intact adult hippocampus: requirement for ERK activation coupled to CREB and upregulation of Arc synthesis. J. Neurosci. *22*, 1532–1540.

EXTENDED EXPERIMENTAL PROCEDURES

Plasmids

Rat CaMKIIα cDNA was amplified from a rat cDNA library by PCR and subcloned into pcDNA3 (Invitrogen). Rat CaMKIIβ in pcDNA3 was a generous gift from Dr. H. Schulman. Rat mEGFP-tagged CaMKIIβe isoform cDNA was a kind gift from Dr. K.U. Bayer at University of Colorado. The mCherry cDNA was generously offered by Dr. R.Y. Tsien (HHMI and UCSD). Point mutants were generated using the QuikChange Site-Directed Mutagenesis Kit (Stratagene). For "rescue" experiments, four silent mutations were introduced into the shRNA target sequence of pcDNA3-CaMKIIβ to generate an shRNA-resistant version of CaMKIIβ (pcDNA3-CaMKIIβres).

For FRET experiments, Arc and CaMKIIβ were fused with improved, monomeric versions of CFP (mCerulean) and YFP (mVenus), respectively, by a transposon-based random insertion method (H.O. and P.F.W., unpublished data), selected by a yeast two-hybrid assay, and subcloned into the pRK5 vector (Genentech). Venus cDNA was a kind gift from Dr. A. Miyawaki of RIKEN-BSI, Japan. The Cerulean cDNA was generated by introducing mutations into pECFP-C1 according to Rizzo et al. (Rizzo et al., 2004). An A206K mutation was introduced into Venus and Cerulean to generate the monomeric versions of these fluorescent proteins (Zacharias et al., 2002). Similarly, the monomeric Venus cDNA was fused with CaMKIIα and Homer1c cDNAs to make pcDNA3-CaMKIIα-mVenus and pcDNA3-Homer1c-mVenus, respectively. The mCerulean-tagged Arc cDNA was then subcloned into the pTRE-tight vector (Clontech) to make pTRE-Arc-mCerulean. The reverse tetracycline-transactivator (rtTA) was excised from pTet-ON (Clontech) and subcloned into a CAG promoter vector to make pCAG-TetON.

A plasmid encoding GFP-tagged tetanus toxin light chain (TeNT) under the control of a doxycycline-inducible promoter was a kind gift from Dr. M. Yamamoto (Mitsubishi Tanabe Pharma Corporation) (Yamamoto et al., 2003). For live imaging of Arc dendritic targeting, an activity-inducible mEGFP-Arc construct was generated by inserting a monomeric EGFP cDNA into the mouse *Arc* cDNA with its 5′ and 3′ untranslated regions (UTRs) under the control of the Arc7000 promoter (pGL4.11-Arc7000-mEGFP-Arc-UTRs) (Kawashima et al., 2009). The same plasmid was linearized and used for the production of mEGFP-Arc Tg mice (see below). The mEGFP-Arc cDNA in the pGL vector was replaced with an mCherry-Arc cDNA to produce pGL4.11-Arc7000-mCherry-Arc-UTRs. All constructs were verified by sequencing.

Antibodies

The primary antibodies used in the present study were mouse anti-PSD-95 monoclonal antibody (mAb) (clone 6G6-1C9, 1:2000, Affinity BioReagents and Millipore), rat anti-GFP mAb (GF90R, 1:4000, NacalaiTesque, Kyoto, Japan), rabbit anti-GFP polyclonal antibody (pAb) (Invitrogen), mouse anti-CaMKIIα mAb (CBα-2, 1:1000, Invitrogen), and anti-CaMKIIβ mAb (CBβ-1, 1:2000, Invitrogen). Rabbit anti-Arc pAb (OP-1 and OP-2) were raised against bacterially expressed recombinant GST-fused full-length Arc, and affinity-purified using beads conjugated with maltose-binding protein (MBP)-Arc (Kawashima et al., 2009). The specificity of the Arc antibodies were confirmed by an antigen-absorption experiment in which Arc antibodies that were pre-absorbed with a 100-fold excess amount of MBP-Arc was used for immunostaining (Figure S2C). Mouse mAbs for Arc were also used for some experiments (either from Santa Cruz or made at Johns Hopkins University). The affinity-purified goat anti-vGlut1 pAb was a kind gift from Dr. M. Watanabe at Hokkaido University (Miyazaki et al., 2003). Goat and donkey AlexaFluor405-, AlexaFluor488-, AlexaFluor555-, AlexaFluor594-, and AlexaFluor647-conjugated anti-mouse, anti-rabbit, anti-goat, and anti-rat IgG antibodies (Invitrogen) were used for secondary fluorescence detection for immunocytochemistry and immunohistochemistry.

Primary Neuronal Cultures

Hippocampal neurons were prepared from the CA1/CA3 regions of the hippocampus of 1-day-old (P1) Sprague Dawley rats as described elsewhere (Bito et al., 1996; Kawashima et al., 2009; Redondo et al., 2010; Takemoto-Kimura et al., 2007). Briefly, the cells were plated on Matrigel (Invitrogen)-coated coverslips or glass-bottom dishes, and cultured in minimal essential medium (MEM) supplemented with 1 mM Glutamax-I, 25 μg/ml insulin, 2% B-27 supplement, and 5% fetal calf serum. Dentate gyrus (DG) granule cells were prepared from hippocampal dentate gyri of P1 rats and cultured on poly-L-lysine/Matrigel-coated coverslips in the culture medium. Glial proliferation was suppressed by adding 4 μM cytosine arabinoside (Sigma) to the medium 2 days after plating. At 14-24 days in vitro (DIV), the cells were incubated in a growth medium containing TTX (2 μM, Wako, Osaka, Japan) for 24 hr. The hippocampal CA neurons (CA pyramidal cells) were then treated with BDNF (50 ng/ml, generously provided by Dainippon Sumitomo Pharma Co., Ltd., Osaka, Japan) for 2 hr, further treated with a medium containing channel blockers or inhibitors, and then fixed for immunostaining. For activation of DG granule cells, a cocktail containing 4-aminopyridine (4AP, 100 μM), bicuculline (BIC, 30 μM), strychnine (1 μM) and glycine (100 μM) was used (referred to as BIC/4AP in the text and figures).

All animal experiments were carried out in accordance with the regulations and guidelines for the care and use of experimental animals at the University of Tokyo and Niigata University and were approved by the institutional review committees of the University of Tokyo Graduate School of Medicine and Niigata University Brain Research Institute.

Yeast Two-Hybrid Screening

Arc-interacting proteins were identified using yeast two-hybrid screening, as described previously (Chowdhury et al., 2006). Briefly, the full-length Arc open reading frame was subcloned into the yeast expression vector pPC97. A random-primed cDNA library was prepared from rat seizure-stimulated cerebrum and cloned into the expression vector pPC86. Then, 1×10^6 cDNAs were screened in

yeast strain HF7c cells (Clontech). Yeast cells were transformed using the lithium acetate method. Interacting proteins were identified by colony selection on plates lacking leucine, tryptophan, and histidine and confirmed using a β-galactosidase assay.

Western Blotting and Immunoprecipitation

Western blotting was performed essentially as described previously (Chowdhury et al., 2006; Kawashima et al., 2009). Cells were lysed in an SDS sample buffer and separated on a standard discontinuous SDS-polyacrylamide gel (10%) or on a gradient polyacrylamide gel (4%–12%) (Invitrogen). The anti-Arc pAb, anti-GFP pAb, anti-CaMKIIα mAb, anti-CaMKIIβmAb, and anti-β-tubulin mAb (TUB2.1, Sigma) were used as primary antibodies, and horseradish peroxidase (HRP)-conjugated anti-mouse, anti-rabbit antibodies (GE Healthcare) or TrueBlot antibodies (eBioscience) were used as secondary antibodies. Chemiluminescence was detected using ECL-Plus reagent (GE Healthcare) and a LAS4000mini image analyzer (Fujifilm).

Immunoprecipitation was performed essentially as described previously, with some modifications (Chowdhury et al., 2006). Crude synaptosomal (P2) fractions were prepared from mouse brains and solubilized with 0.1% NP-40. Total brain lysates were also prepared from the mouse forebrain by homogenization in a standard RIPA buffer followed by sonication and clarification by centrifugation. For heterologous cell lysates, HEK293T cells were transfected with mammalian expression vectors for either Arc or CaMKIIβ, or both, and sonicated in a lysis buffer. The protein concentrations of the lysates were measured by either the BCA (Pierce) or Bradford (Bio-Rad) method. The lysates were preabsorbed with nProteinA-sepharose beads (GE Healthcare) and then incubated with the anti-CaMKIIβmAb in a binding buffer containing 50 mM Tris-Cl (pH7.5), 150 mM NaCl, 5% Glycerol, 1mM DTT, 0.1% NP-40, 1mM EDTA and protease inhibitors. The immune complex was captured with nProteinA-sepharose beads and washed with a binding buffer using chromatography micro-columns (Bio-Rad). The immunoprecipitates were eluted with an SDS sample buffer and analyzed by Western blotting.

Purification of Recombinant Proteins and In Vitro Binding

The expression and purification of GST-fusion proteins were performed essentially as described previously (Chowdhury et al., 2006). Briefly, the rat full-length *Arc* cDNA was subcloned into the pGEX4T-2 vector (GE Healthcare), and GST-Arc and GST were expressed in BL21-Gold bacterial cells (Stratagene). GST-Arc was also expressed using the baculovirus-insect cell expression system (Invitrogen). The cells were harvested and lysed in PBS containing a protease inhibitor cocktail (Complete, Roche). The cell lysates were cleared by ultracentrifugation (100,000 x *g*) and incubated with glutathione-sepharose 4B beads (GE Healthcare). After several washes with PBS, GST proteins were eluted with 10 mM glutathione/50 mM Tris-Cl (pH 8.0) and desalted with PD-10 columns (GE Healthcare). MBP-fused Arc was expressed and purified using a kit (pMAL protein fusion and purification system, New England BioLabs).

Recombinant CaMKII and its mutant proteins were expressed in mammalian cells. HEK293T cells were transfected with CaMKII cDNAs in the pcDNA3 vector. Forty-eight hours after transfection, the cells were harvested and lysed in Tris-buffered saline (TBS, pH 7.5) containing 1 mM DTT, 0.1 mM EGTA, 0.02% Triton X-100 and a proteinase inhibitor cocktail (Complete, Roche). The cell lysates were cleared by ultracentrifugation (100,000 x *g*); 1 mM $CaCl_2$ was then added to the supernatant, which was then incubated with calmodulin-sepharose 4B beads (GE Healthcare). The beads were washed with a binding buffer, and bound proteins were eluted with TBS containing 1 mM EGTA. The eluted fractions were concentrated by ultrafiltration (Amicon Ultra15, Millipore) and desalted with PD-10 columns. Integrity and purity of the purified recombinant CaMKII samples were confirmed by a Coomassie Brilliant Blue staining (Figure S1D). Protein concentration was measured by either the BCA (Pierce) or Bradford (Bio-Rad) method.

For in vitro binding assays, glutathione-sepharose 4B beads were incubated with GST or GST-Arc in PBS for 1 hr at room temperature. The glutathione-sepharose beads were washed and incubated with purified recombinant CaMKII proteins in a binding buffer containing 20 mM Tris-Cl (pH 7.4), 150 mM NaCl, 5% glycerol, 0.1% (for CaMKIIβ) or 0.02% (for CaMKIIα) NP-40, and 1 mM dithiothreitol. For Ca^{2+}/CaM-plus conditions, 2 μM calmodulin (Calbiochem) and 2 mM $CaCl_2$ were added to the reaction mixtures, whereas 2 mM EGTA was added for Ca^{2+}-free conditions. After incubation for 1 hr, the beads were washed with binding buffer, and bound proteins were eluted with an SDS sample buffer. The eluted samples were analyzed by SDS-PAGE followed by Western blotting. After treated with horseradish peroxidase-conjugated secondary antibodies, chemiluminescent reagents (ECL-Plus, GE Healthcare, or Immobilon Western, Millipore) were used for luminescence signal development. The signals were visualized and quantified using luminescence analyzing systems (FAS-1000, Toyobo, Japan, or LAS-4000mini, Fuji, Japan) or X-ray films. We sometimes observed slowly migrated bands in Western blots of GST-pull-down assay, especially when the binding reactions contained EGTA to minimize free Ca^{2+}. SDS-resistant multimers of CaMKII were previously shown to become detectable under oxidizing conditions in vitro (Shetty et al., 2008).

Immunocytochemistry

Neuron cultures were immunostained essentially as described previously (Kawashima et al., 2009; Nonaka et al., 2006; Redondo et al., 2010; Takemoto-Kimura et al., 2007). Briefly, the cells were fixed in 4% paraformaldehyde/4% sucrose/phosphate-buffered saline (PBS), washed with PBS, and permeabilized with 0.3% Triton X-100/PBS. The cells were incubated in a blocking buffer (5% normal goat serum or normal donkey serum, 3% BSA and 0.3% Triton X-100 in PBS), and then incubated with primary antibodies. The primary antibodies were detected with Alexa Fluor-conjugated secondary antibodies. A post fixation with 4%

paraformaldehyde was applied. Immunostained coverslips were nuclear-stained with DAPI or Hoechst33342, if applicable, and mounted on slides for microscopic analyses.

RNAi Knockdown

Short-hairpin (sh) RNA vectors for CaMKIIα (sh α), CaMKIIβ (sh β), and a negative control (sh nega) were constructed in pSUPERneo+GFP (OligoEngine) as described previously (Takemoto-Kimura et al., 2007). The target sequences used were 5′-GGATCTGATCAATAAGATG-3′ (nucleotides 735-753 of CaMKIIα), 5′-GCCAAGAGTTTACTCAACA-3′ (nucleotides 1021–1039 of CaMKIIβ), and 5′-ATCCGCGCGATAGTACGTA-3′ (for sh nega). Hippocampal CA1/CA3 neurons were transfected with shRNA vectors using Lipofectamine 2000 (Invitrogen) at 10-11 DIV and then treated with TTX for 24 hr at 15-17 DIV. The cells were then treated with BDNF for 2 hr followed by TTX for 2 hr to induce the expression and accumulation of endogenous Arc in dendritic spines. Neurons were fixed, immunostained for GFP, Arc, and CaMKIIβ and then subjected to a spine accumulation assay (see below). For ''rescue'' experiments, the shRNA-resistant CaMKIIβ constructs (wild-type and mutant cDNAs in pcDNA3) were cotransfected with the pSUPER-sh β vector. Specific knockdown for the α- and β-isoforms of CaMKII were confirmed by immunostaining and quantification (Figure S5B). For a control, shRNA vector-transfected cells were immunostained with a Pan-anti-Homer pAb (Tu et al., 1998) and analyzed for Homer accumulation in dendritic spines.

Image Acquisition and Analyses of Immunostained Neurons

Wide-field fluorescence images were obtained using a color CCD camera (DP-70, Olympus, Tokyo, Japan) attached to an upright microscope (BX-51, Olympus) or an EM-CCD camera (iXon, Andor) attached to an inverted microscope (IX81, Olympus). Confocal fluorescence images were obtained using a confocal laser microscopy system (LSM 510META-V3.2, Carl Zeiss) built on an inverted microscope (Axiovert 200M, Carl Zeiss). Confocal z-stack images of dendritic segments (0.5-1 μm intervals, 4-6 images/stack) were obtained using a 63x objective (NA 1.4, oil) with a scan zoom of 6 and analyzed offline using MetaMorph software (Molecular Devices). All stacked images were projected into single planes by summation and used for quantitative analyses as described below.

For the evaluation of Arc localization in the PSD (Figures 2A, S2, and S3), PSD spots were defined on the basis of PSD-95 IR clustering essentially as described previously (Nonaka et al., 2006). All PSD-95 spots that were well-separated from the dendritic shaft of an Arc-IR positive dendrite were analyzed, and a corresponding non-PSD area that was adjacent to a given PSD spot was defined within dendritic shafts for each PSD spot. After background subtraction, the average intensity of Arc immunofluorescence was measured. The intensity ratio of PSD to non-PSD was designated as the Arc accumulation index. Image acquisition and offline calculations were performed by a person who was blinded to the culture conditions.

In the TeNT experiment (Figures 2C and S3D), the axons that were expressing GFP-TeNT were traced and their crossing points with the Arc-IR positive dendrites were identified. If a PSD-95-IR positive spot that protruded from the dendritic shaft was found to be juxtaposed or overlaid with a GFP-IR positive axon at the crossing point, the PSD-spot was defined as the ''GFP^+'' spine. Surrounding GFP-IR negative PSD-spots (within ~10 μm) in the same dendrite were defined as ''GFP^-'' spines, and the mean intensity of Arc IR across all GFP^- spines was calculated. The ratio of the Arc IR intensity in the GFP^+ spine to the mean IR intensity in the GFP^- spines was then calculated (GFP^+/GFP^- ratio). Similar measurements were performed for GFP-expressing axons as the control. GFP-TeNT and GFP were induced in neurons using a doxycycline-inducible system (Clontech). Essentially the same procedure was applied to analyze surface GluA1 and Arc-IR levels in experiments shown in Figures S4B and S4D. Types of vectors that were transfected to neurons were coded and image acquisition/analyses were performed in a blind manner.

For RNAi experiments (Figures 5, S5, and S6), dendritic segments from GFP (a marker of the shRNA vectors) and Arc double-positive neurons were imaged. CaMKIIβ knockdown and RNAi-resistant CaMKIIβ expression were confirmed by simultaneous CaMKIIβ immunostaining. Dendritic spine accumulation was evaluated by analyzing the fluorescence-intensity profiles of dendrites. Briefly, for each dendritic spine identified with a GFP-IR signal, the fluorescence intensities of Arc and GFP IR were measured along a straight line that crossed the spine and the adjacent dendritic shaft, and intensity peaks were obtained in both spine and shaft regions. The spine index for Arc was defined as follows:

$$\text{Spine index} = \frac{(\text{Arc-IR peak intensity in spine}/\text{Arc-IR peak intensity in shaft})}{(\text{GFP-IR peak intensity in spine}/\text{GFP-IR peak intensity in shaft})}.$$

The spine index for Homer was also analyzed using similar procedures. The types of sh vectors that were transfected to neurons were coded, and image acquisition and analyses were performed in a blind manner.

Measurement of Fluorescent Resonance Energy Transfer

Hippocampal CA1/CA3 neurons cultured on glass-bottom dishes (MatTek Corporation) were cotransfected with pTRE-Arc-mCerulean, pCAG-TetON and pRK5-CaMKIIβ-mVenus at a ratio of 2:1:2 at 7-8 DIV. The pcDNA3-CaMKIIα-mVenus, pcDNA3-Homer1c-mVenus or pCMV-mVenus was used in place of the CaMKIIβ-mVenus plasmid as a control. The CFP-tagged Arc was induced by adding doxycycline (2 μg/ml) at 18-22 DIV for 24 hr before starting live imaging. TTX (1μM) was also added to the culture medium. Fluorescent images of the dendritic shafts were obtained from living neurons using a Zeiss LSM510 confocal microscope, equipped with a stage CO_2 incubator (Tokai Hit). Fluorescent resonance energy transfer (FRET) was measured with the donor

dequenching after acceptor photobleaching method as described previously (Takemoto-Kimura et al., 2007). CFP and YFP signals were monitored by independent scans using 458 nm light and 514 nm light as excitation with 470-500 nm (for CFP) and 530-600 nm (for YFP) band-pass filters, respectively. Acceptor photobleaching was achieved by repetitive scans with intense 514 nm laser light on dendritic regions of transfected neurons. Regions of interest (ROIs) for quantification were set on the head of dendritic spines. After background subtraction, FRET efficiency was calculated as follows:

$$FRET\ Efficiency(\%) = \frac{(F_{CFP,\ after} - F_{CFP,\ before}) \times 100}{F_{CFP,\ after}}$$

where $F_{CFP,\ before}$ and $F_{CFP,\ after}$ represent the averaged CFP fluorescent signals before and after the YFP photobleaching, respectively (Takemoto-Kimura et al., 2007).

In our measurements (Figure S1C), the FRET efficiency between Arc-CFP and CaMKIIβ-YFP was relatively low. Nonetheless, the efficiency was significantly higher than the theoretical null value of zero ($p < 0.0001$), and also than values of other control FRET pairs we used ($p < 0.001$, versus Homer1c-YFP ; $p < 0.01$, versus CaMKIIα-YFP). Such inefficiency in FRET could be due to a non-optimal donor/acceptor expression ratio and/or sub-optimal orientation of donor and acceptor dipoles.

FP-Tagged Arc Live Imaging

For monitoring dendritic targeting of Arc protein, hippocampal neurons plated on glass-bottom dishes (MatTek) were co-transfected with the pGL4.11-Arc7000-mEGFP-Arc-UTRs and a marker plasmid pTagRFP-C (Evrogen) (Figure 3A), or pGL4.11-Arc7000-mCherry-Arc-UTRs and pcDNA3-mEGFP-CaMKII (Figure 3C) at 7-9 DIV. At 16-22 DIV, neurons in the dishes were incubated in a culture medium containing BDNF (50 ng/ml) for 2 hr and then, just prior to the start of live imaging, the medium was replaced with conditioned medium containing TTX (1 μM) or medium without any inhibitors. Fluorescent images of dendritic shafts were obtained from living neurons using a Zeiss LSM510 laser scanning confocal microscope with excitation at 488 nm for GFP and at 543 nm for RFP. Series of z-stack images for both GFP and RFP signals were acquired in time-lapse mode. The neurons were maintained at 37°C in a stage CO_2 incubator (Tokai Hit, Japan) during imaging sessions.

Images were quantitatively analyzed using the MetaMorph software. The z-stack images were projected into a single-plane image by summation, and the fluorescence line profiles of well-separated spines and adjacent dendritic shafts were measured. Only the spines that were consistently present during an imaging session were included in the analysis. Similar to the shRNA experiments, an index for spine accumulation was defined as follows:

$$\text{Spine index} = \frac{(GFP_{spine}/GFP_{shaft})}{(RFP_{spine}/RFP_{shaft})},$$

where GFP_{spine} and GFP_{shaft} represent the peak green fluorescent intensities, while RFP_{spine} and RFP_{shaft} indicate the peak red fluorescent intensities, in the spine and the shaft, respectively. The spine and shaft regions were defined by the line profile of the filler RFP. The ratios of spine indices before and 2 hr after follow-up incubation of individual spine-shaft pairs were calculated for a cumulative frequency presentation.

Field Electrical Stimulation and Live-Cell Imaging

Hippocampal CA1/CA3 neurons plated on glass-bottom dishes were transfected with pGL4.11-Arc7000-mEGFP-Arc-UTRs, pCaMKIIp-TagRFP and pCaMKIIp-SNAP-GluA1 plasmids at 8 DIV and used for live imaging at 19-23 DIV. During the imaging session, fluorescent images of dendritic shafts were obtained through green (ex480/em535) and red (ex542/em585) channels using an EM-CCD camera (iXon, Andor) equipped on an inverted microscope (IX81, Olympus). The neurons were maintained at 37°C in a stage CO_2 incubator (Tokai Hit) during imaging sessions. After taking baseline images for at least 60 min (3min interval/frame), the neuronal culture was stimulated with trains of high-frequency field electrical pulses (0.5 ms pulses, 100 pluses at 50Hz, 4 times with 5 min intervals) (Bito et al., 1996), through platinum electrodes; the current intensity was set at ~5V/cm, which induced volume expansion of approximately 20%–30% of dendritic spines in a given field of view between the electrodes. Such structural changes were accompanied by enhanced surface GluA1 expression and completely blocked in the presence of AP5 and NBQX in our control experiments (Y.I., H.O., and H.B. unpublished data). Dual color images were recorded at 0.5 min interval/frame for 20 min after the stimulation, and then 4 min interval/frame thereafter. Spine volume was judged as ''expanded'' if the red fluorescence intensity of a spine head averaged across the 1st 10 images after the end of the stimulation (i.e., 15 - 20 min after the onset of the stimulation) exceeded the mean intensity + 2 SD of the last 10 images before the stimulation. The volume-corrected mEGFP-Arc level was defined as a ratio of green fluorescence intensity to red fluorescence intensity. Because the mEGFP-Arc levels considerably differed across neurons due to differential expression levels of TagRFP and mEGFP-Arc in each cell, the mEGFP-Arc levels in the dendritic spines were further standardized by dividing the mean mEGFP-Arc levels in the dendritic shaft for each cell.

Surface AMPA-R Labeling

Extracellular AMPA-Rs were labeled in live hippocampal neurons (17-18 DIV) essentially as described previously (Chowdhury et al., 2006; Shepherd et al., 2006). Briefly, an anti-GluA1 polyclonal antibody (5 μg/ml, Alomone Labs, Jerusalem, Israel) was added to a culture medium followed by incubation at 10°C for 30 min. The unbound excess antibody was quickly washed with a warm culture medium, and the neurons were then fixed with 4% paraformaldehyde/4% sucrose for 20 min at room temperature. The neurons were rinsed with PBS and then incubated with AlexaFluor488-conjugated secondary antibodies under non-permeabilized conditions to stain surface AMPA-Rs. The antibody complex was then further fixed with 4% paraformaldehyde/4% sucrose for 20 min, washed, permeabilized, and treated with a blocking buffer. The neurons were then incubated with an anti-Arc mouse mAb and an anti-vGlut1 guinea pig pAb, washed, and subsequently incubated with anti-mouse IgG AlexaFluor555-conjugated, and anti-guinea pig IgG AlexaFluor647-conjugated secondary antibodies.

The quantification of surface GluA1 puncta was carried out essentially as described previously (Chowdhury et al., 2006; Shepherd et al., 2006) using a custom-made macro running on MetaMorph imaging software (Universal Imaging, Downingtown, PA). Confocal z-stack images of dendritic segments (0.5 μm intervals, 6-10 images/stack) acquired with the LSM510 using a 63x objective (NA 1.4, oil) with a scan zoom of 6 were projected onto single planes by summation. Background signals were subtracted from the projected images, and GluA1 puncta adjacent to vGut1 puncta were selected for analysis. For intensity comparison, mean fluorescent intensities of individual puncta were measured. For correlative analyses between surface GluA1 and synaptic Arc levels, mean Arc IR intensities in the GluA1 puncta were measured in images taken from the samples treated with BDNF followed by TTX. All image analyses were performed by a person who was blinded to the experimental conditions.

In Vivo Analysis of Arc Synaptic Localization Using mEGFP-Arc Tg Mice

The *Arc*-promoter mEGFP-Arc construct was linearized and microinjected into the pronuclei of fertilized C57BL/6 mouse eggs. After screening transgenic (Tg) lines that showed activity-dependent transgene expression in the brain, the line that showed the strongest transgene expression was selected and homozygous animals were used for this study. To investigate GFP-Arc accumulation in the PSD in the brain, adult Tg mice (2 to 5 months old) were dark-reared for 24-28 hr followed by exposure to a bright environment for 4 hr and the injection of TTX into one eye and PBS into the other. The mice were then kept in a bright environment for 2 hr and were subsequently fixed by transcardial perfusion; the brains were removed, cryoprotected, and frozen. The primary visual cortex was sectioned for immunohistochemistry into 25 μm-thick sections using a cryostat. The sections were permeabilized, blocked with 5% normal goat serum, and incubated with a rabbit anti-GFP pAb and a mouse anti-PSD-95 mAb. The primary antibodies were visualized with an AlexaFluor488-conjugated secondary antibody for GFP and an AlexaFluor594-conjugated antibody for PSD-95. Nuclei were counterstained with Hoechst 33342 or 4′,6-diamino-2-phenylindole (DAPI). The side of the TTX-injected eye was randomized for each animal, but the total numbers of injections into each side were balanced over the whole experiment. For each animal, the right and left hemispheres were coded by a person who was blinded to the side of the TTX-injection, and the following quantification was performed in its entire process by another person in a double-blinded manner.

High-power fluorescence z-stack images were taken at a total of six fields of view in the monocular region of the primary visual cortex from three different sections of each hemisphere for each animal using a Zeiss LSM510 with a 63x objective at a scan zoom of 8. GFP-IR signals in the PSD-95 spots were analyzed using a macro function of the MetaMorph software. Briefly, the z-stack images were projected into a single plane by summation. PSD spots were defined as clusters of pixels whose fluorescence intensity was above the mean + 3 SD of the background signal distribution in a PSD-95 image. The average intensity of the raw GFP-IR signal in each PSD spot was measured, and the raw GFP-IR signal distribution was blindly calculated for each hemisphere of each animal without background subtraction. In independent control experiments, the level of background of GFP-IR signals was found to be relatively high and represented about bottom 90% of the GFP-IR signals in the PSD spot. Thus, for each animal, a comparison was made between hemispheres using the mean intensity of the top 10% of the GFP-IR signal distribution in each hemisphere (Figure 6C).

CaMKIIβ Knockout Mice

Gene targeting of CaMKIIβ was carried in the C57BL/6-derived ES cell line RENKA (Mishina and Sakimura, 2007) by homologous recombination. Exons 9 to 11 of the mouse *Camk2b* gene were flanked by LoxP sites and then deleted with Cre-mediated recombination. Detailed characterization of CaMKIIβ null mice will be described elsewhere (K. Sakimura and K.A., unpublished data). Genotypes were identified by PCR with following specific primers: Cmk2b5R (5′-TGGTCTGGACTTGCAAACAG-3′) and Cmk2bgt1 (5′-GAGATGGAGCAGGGATCAGA-3′). The approximate lengths of the amplified DNA fragments are 0.96 kbp for wild-type and 170 bp for null. Heterozygous CaMKIIβ mutant mice were crossed with the mEGFP-Arc Tg mice to produce CaMKIIβ-heterozygous mutant/mEGFP-Arc Tg mice, which were subsequently used to generate CaMKIIβ-KO/mEGFP-Arc mice.

SUPPLEMENTAL REFERENCES

Bito, H., Deisseroth, K., and Tsien, R.W. (1996). CREB phosphorylation and dephosphorylation: a Ca(2+)- and stimulus duration-dependent switch for hippocampal gene expression. Cell *87*, 1203–1214.

Chowdhury, S., Shepherd, J.D., Okuno, H., Lyford, G., Petralia, R.S., Plath, N., Kuhl, D., Huganir, R.L., and Worley, P.F. (2006). Arc/Arg3.1 interacts with the endocytic machinery to regulate AMPA receptor trafficking. Neuron *52*, 445–459.

Kawashima, T., Okuno, H., Nonaka, M., Adachi-Morishima, A., Kyo, N., Okamura, M., Takemoto-Kimura, S., Worley, P.F., and Bito, H. (2009). Synaptic activity-responsive element in the Arc/Arg3.1 promoter essential for synapse-to-nucleus signaling in activated neurons. Proc. Natl. Acad. Sci. USA *106*, 316–321.

Mishina, M., and Sakimura, K. (2007). Conditional gene targeting on the pure C57BL/6 genetic background. Neurosci. Res. *58*, 105–112.

Miyazaki, T., Fukaya, M., Shimizu, H., and Watanabe, M. (2003). Subtype switching of vesicular glutamate transporters at parallel fibre-Purkinje cell synapses in developing mouse cerebellum. Eur. J. Neurosci. *17*, 2563–2572.

Nonaka, M., Doi, T., Fujiyoshi, Y., Takemoto-Kimura, S., and Bito, H. (2006). Essential contribution of the ligand-binding beta B/beta C loop of PDZ1 and PDZ2 in the regulation of postsynaptic clustering, scaffolding, and localization of postsynaptic density-95. J. Neurosci. *26*, 763–774.

Redondo, R.L., Okuno, H., Spooner, P.A., Frenguelli, B.G., Bito, H., and Morris, R.G. (2010). Synaptic tagging and capture: differential role of distinct calcium/calmodulin kinases in protein synthesis-dependent long-term potentiation. J. Neurosci. *30*, 4981–4989.

Rizzo, M.A., Springer, G.H., Granada, B., and Piston, D.W. (2004). An improved cyan fluorescent protein variant useful for FRET. Nat. Biotechnol. *22*, 445–449.

Shepherd, J.D., Rumbaugh, G., Wu, J., Chowdhury, S., Plath, N., Kuhl, D., Huganir, R.L., and Worley, P.F. (2006). Arc/Arg3.1 mediates homeostatic synaptic scaling of AMPA receptors. Neuron *52*, 475–484.

Shetty, P.K., Huang, F.L., and Huang, K.P. (2008). Ischemia-elicited oxidative modulation of Ca^{2+}/calmodulin-dependent protein kinase II. J. Biol. Chem. *283*, 5389–5401.

Takemoto-Kimura, S., Ageta-Ishihara, N., Nonaka, M., Adachi-Morishima, A., Mano, T., Okamura, M., Fujii, H., Fuse, T., Hoshino, M., Suzuki, S., et al. (2007). Regulation of dendritogenesis via a lipid-raft-associated Ca^{2+}/calmodulin-dependent protein kinase CLICK-III/CaMKIgamma. Neuron *54*, 755–770.

Tu, J.C., Xiao, B., Yuan, J.P., Lanahan, A.A., Leoffert, K., Li, M., Linden, D.J., and Worley, P.F. (1998). Homer binds a novel proline-rich motif and links group 1 metabotropic glutamate receptors with IP3 receptors. Neuron *21*, 717–726.

Yamamoto, M., Wada, N., Kitabatake, Y., Watanabe, D., Anzai, M., Yokoyama, M., Teranishi, Y., and Nakanishi, S. (2003). Reversible suppression of glutamatergic neurotransmission of cerebellar granule cells in vivo by genetically manipulated expression of tetanus neurotoxin light chain. J. Neurosci. *23*, 6759–6767.

Zacharias, D.A., Violin, J.D., Newton, A.C., and Tsien, R.Y. (2002). Partitioning of lipid-modified monomeric GFPs into membrane microdomains of live cells. Science *296*, 913–916.

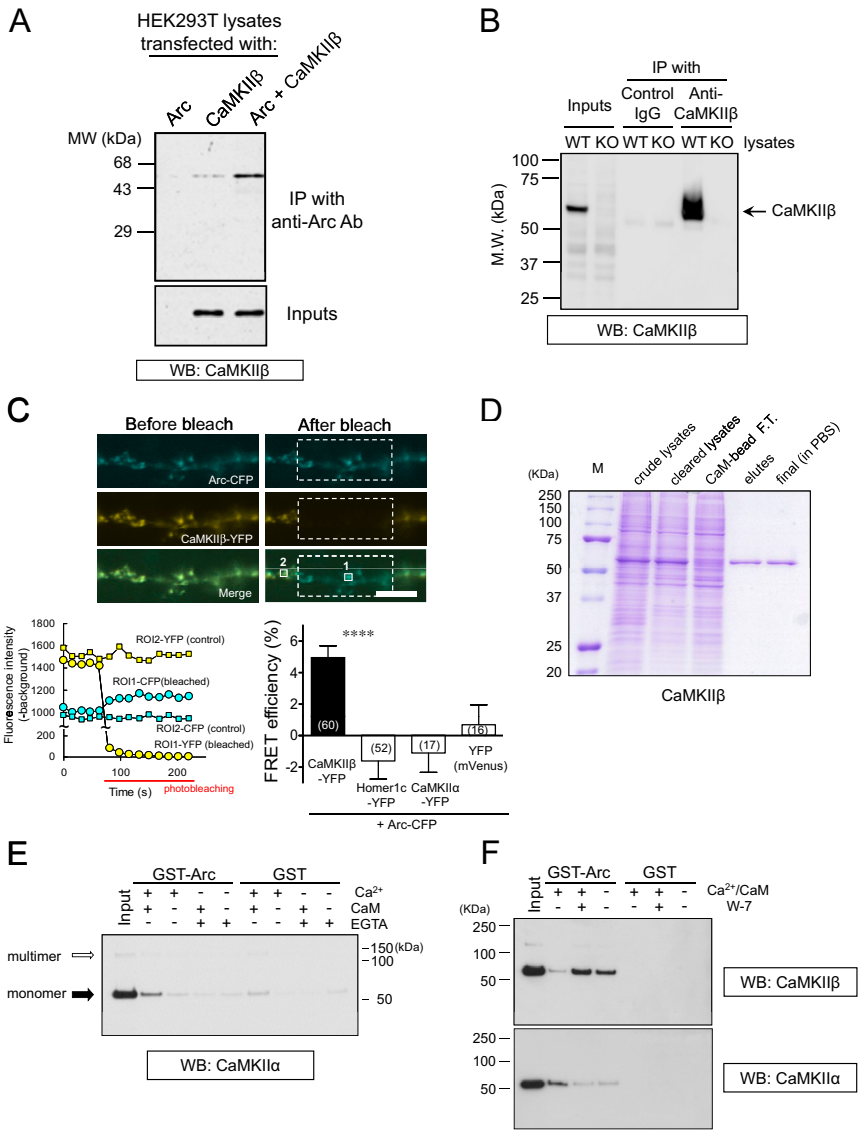

Figure S1. Arc and CaMKIIβ Make a Complex In Vitro, Related to Figure 1

(A) Co-immunoprecipitation of Arc and CaMKIIβ in lysates from transfected HEK293T cells. The lysates were analyzed by co-immunoprecipitation with an anti-Arc pAb and by probing with anti-CaMKIIβ.

(B) Brain co-immunoprecipitates shown in Figure 1B were probed with the anti-CaMKIIβ antibody.

(C) FRET analysis of Arc interaction with CaMKIIβ in dendritic spines of living neurons that were treated with TTX. CFP fluorescence was measured in spines inside (ROI 1) and outside (ROI 2) the acceptor photo-bleached area (dotted frames), and plotted in a graph at the bottom left. The mean FRET efficiency calculated from the CFP de-quenching was shown at the bottom right. Several control constructs were included. The numbers in parentheses in the bars represent the total numbers of spines examined. ****$p < 0.0001$ by one-sample t test versus the theoretical null value of zero. Error bars represent SEM.

(D) Purification of recombinant CaMKIIβ. A representative SDS-PAGE gel stained with Coomassie Brilliant Blue (CBB) is shown. Recombinant CaMKIIβ was expressed in HEK293T cells and purified using CaM-beads. F.T., flowthrough.

(E) Interaction between Arc and CaMKIIα in the presence of Ca^{2+}/CaM.

(F) Inhibition of CaM activation by W-7 (100 μM) in the presence of Ca^{2+}/CaM restored Arc binding to CaMKIIβ (top). The Ca^{2+}/CaM dependency of Arc-CaMKIIα binding was also confirmed by W-7 treatment (bottom).

IP, immunoprecipitation; WB, western blot.

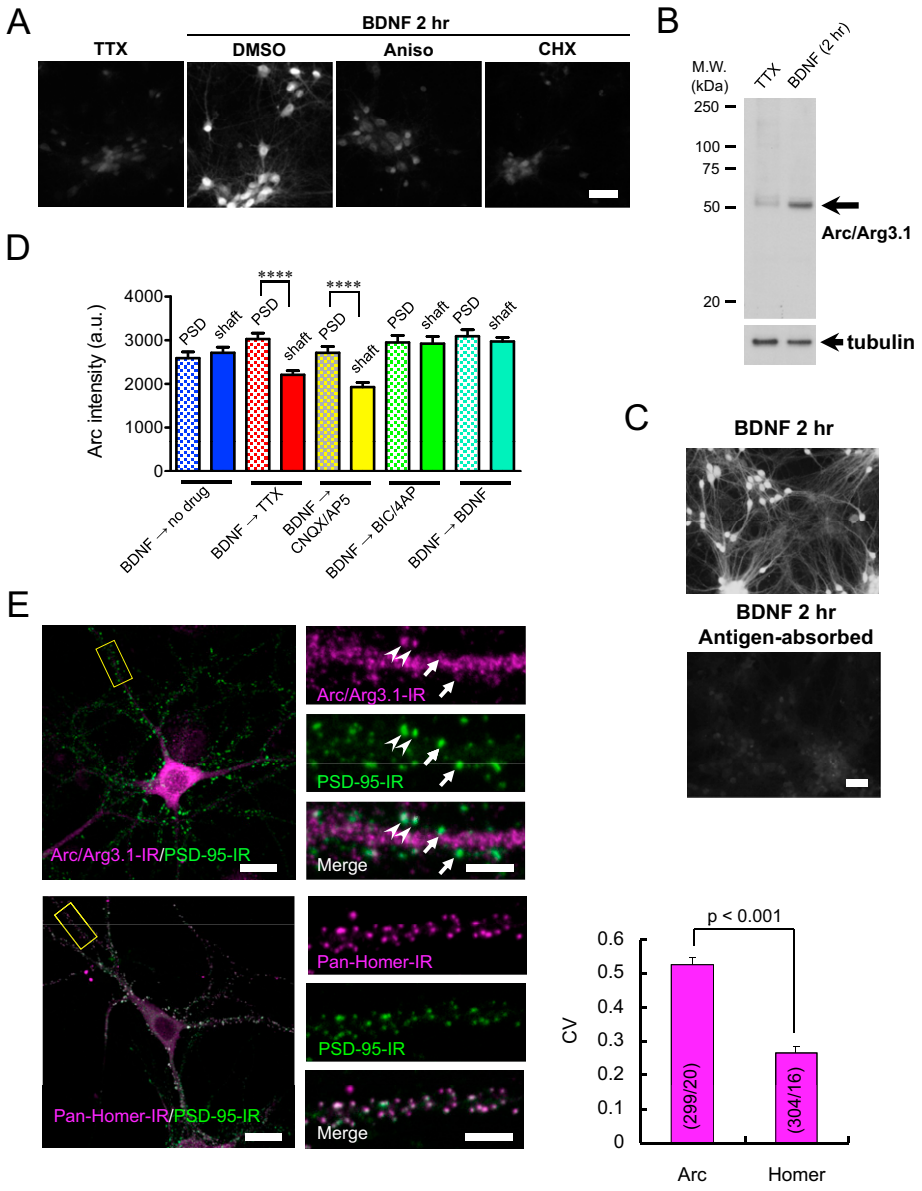

Figure S2. Activity-Dependent Arc Protein Synthesis in Cultured Hippocampal Pyramidal Neurons, Related to Figure 2

(A) Protein synthesis inhibitors blocked BDNF-induced Arc expression in hippocampal neurons. Cultured neurons were treated with anisomycin (20 μM) or cycloheximide (50 μg/ml) and immunostained for Arc to confirm that BDNF-induced Arc is dependent on new protein synthesis. Scale bar, 50 μm.

(B) BDNF-induced Arc was analyzed by Western blot. A specific band of 52-55 kDa was detected.

(C) The specificity of an anti-Arc antibody used in this study was confirmed by antigen absorption. After anti-Arc antibody was pre-absorbed with recombinant full-length Arc, it failed to label any BDNF-treated hippocampal neurons. Scale bar, 50 μm.

(D) Average absolute intensities of the immunofluorescent signals for Arc at the PSD and at the dendritic shaft in hippocampal cultures treated with BDNF followed by synaptic suppression or activation. The same dataset shown in Figure 2B is displayed in a different format to show the absolute values before index calculation. ****$p < 0.0001$ by ANOVA with a post hoc paired test. The numbers of PSD puncta (n) and cells (N) analyzed were n = 210 (N = 17) for BDNF → no drugs, n = 187 (N = 19) for BDNF → TTX, n = 152 (N = 12) for BDNF → BIC/4AP, n = 205 (N = 19) for BDNF → CNQX/APV, and n = 120 (N = 12) for BDNF → BDNF.

(E) Enhanced variability of Arc content in individual synapses in comparison with Homer. Left top, representative Arc-IR and PSD-95-IR in a hippocampal neuron kept in a normal culture medium without inhibiters. The framed area (yellow box) at left is expanded and shown in separate channels at right. Across spines identified by PSD-95, Arc content fluctuated from high (arrowheads) to very low levels (arrows). Left bottom panels, representative images of Homer in a hippocampal neuron kept in a basal culture medium. Scale bars, 20 μm and 5 μm. Right, A bar graph for a mean coefficient of variance (CV) analysis. The numbers in parentheses in the bars represent the total numbers of dendritic segments and cells (segments/cell) examined. The p value represents the statistical significant level by unpaired t test.

Error bars represent SEM.

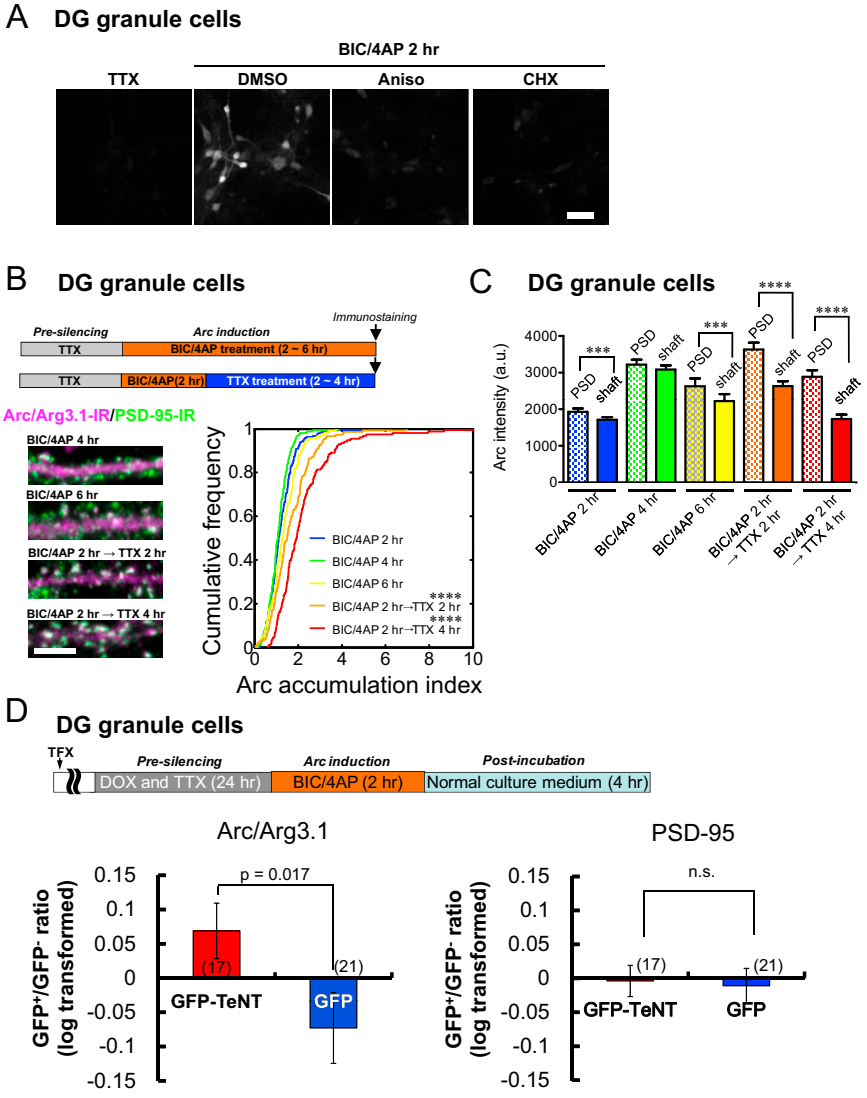

Figure S3. The Spine Localization of Arc Is Modulated by Synaptic Inactivity in DG Granule Cells, Related to Figure 2

(A) Protein synthesis inhibitors blocked BIC/4AP-induced Arc expression in DG granule cells. Immunostaining for Arc was performed in a similar fashion to Figure S2A, except that DG neurons were activated with BIC/4AP for 2 hr. BIC/4AP-induced Arc also depended on new protein synthesis. Scale bar, 50 μm.

(B) Accumulation of Arc in spines is induced by synaptic inactivity that follows strong synaptic activity in DG granule cells. A schematic diagram of the culture treatment is shown on the top. Scale bar, 5 μm. A cumulative frequency histogram of Arc accumulation index is shown at the bottom right. The numbers of PSD puncta (n) and cells (N) analyzed were n = 188 (N = 20) for BIC/4AP 2 hr, n = 165 (N = 18) for BIC/4AP 4 hr, n = 148 (N = 16) for BIC/4AP 2 h → TTX 2 hr, n = 118 (N = 16) for BIC/4AP 6 hr, and n = 156 (N = 17) for BIC/4AP 2 h → TTX 4 hr. ****p < 0.0001 when compared with BIC/4AP 2 hr by a K-S test.

(C) Average absolute intensities of the immunofluorescent signals for Arc in DG neurons treated with BIC/4AP followed by TTX. The same dataset shown in panel B is displayed in a different format to show the absolute values before index calculation. ***p < 0.001; ****p < 0.0001 by ANOVA with a post hoc Tukey's test.

(D) Suppression of single-synapse activity was performed using DOX-inducible GFP-TeNT in a similar manner to that described in Figures 2C–2E, except that DG neurons and a BIC/4AP activation protocol were used here. In accordance with the results from hippocampal neurons, enrichment of the GFP^+/GFP^- ratio for Arc was detected with the GFP-TeNT condition but not with the GFP control. The GFP^+/GFP^- ratio of PSD-95 did not differ between GFP-TeNT and GFP control conditions. The p value represents the statistical significant level by t test.

Error bars represent SEM. n.s., not signficant.

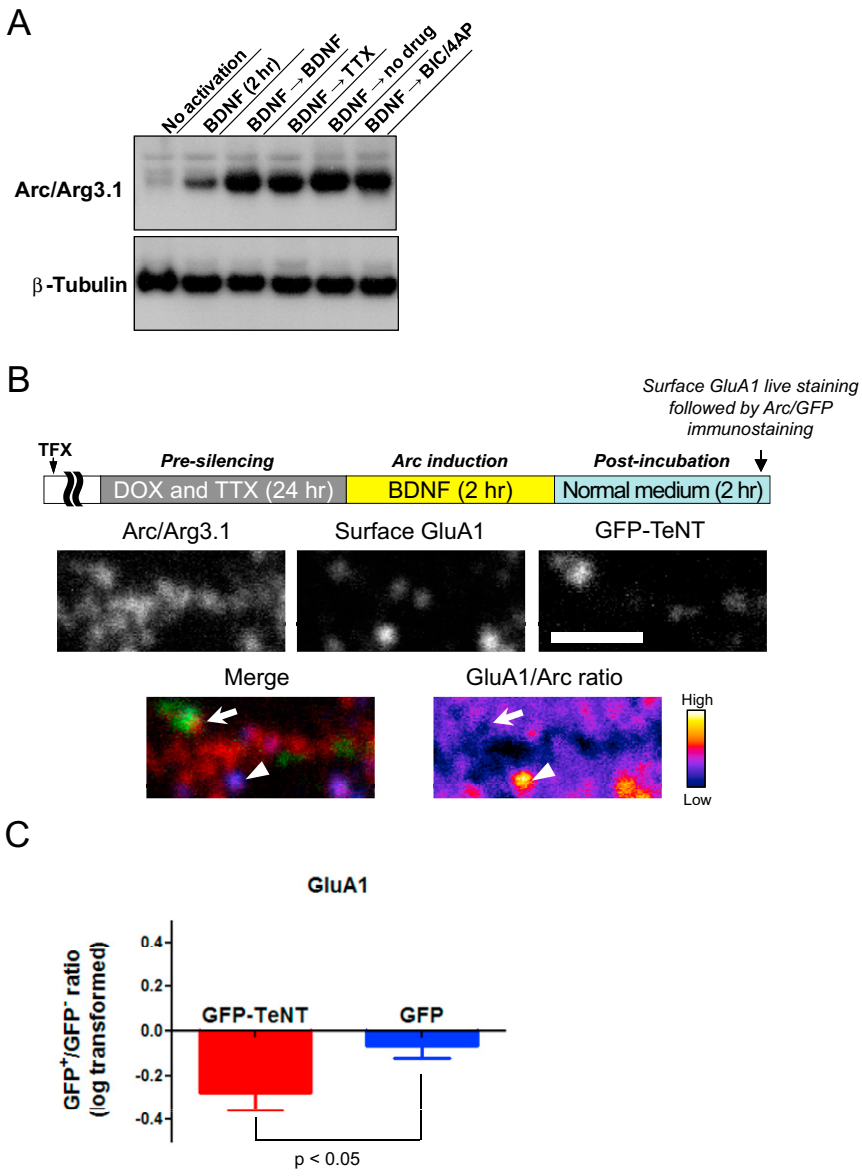

Figure S4. Overall Arc Expression in Hippocampal Culture, Related to Figure 4

(A) A representative Western blot for Arc is shown. Lysates were prepared from hippocampal culture dishes that were treated with BDNF followed by various pharmacological manipulations. The overall Arc protein levels were dramatically increased by BDNF treatment for 2 hr followed by the 2-h periods of pharmacological manipulations. At 4 hr, the BDNF-induced Arc levels were similar among groups, regardless of pharmacological manipulations. Similar results were obtained in replicated experiments.

(B) Suppression of single-synapse activity was carried out using DOX-inducible GFP-TeNT in essentially the same manner as used in Figures 2 and S3, except that surface GluA1 and synaptic Arc levels were visualized here. Arrows and arrowheads indicate Arc-rich/GluA1-poor and Arc-poor/GluA1-rich spines, respectively. A pseudo-color ratiometric image of GluA1/Arc was also shown. Scale bar, 2 μm.

(C) A bar graph of the GFP^+/GFP^- ratio of GluA1. The ratiometric values were log transformed. The GFP^+/GFP^- ratio of GFP-TeNT was significantly lower than that of the GFP control ($p < 0.05$). The GFP^+/GFP^- ratio for Arc was significantly higher in the GFP-TeNT condition than in the GFP control, replicating the results shown in Figures 2D and S3D (not shown).

Error bars represent SEM.

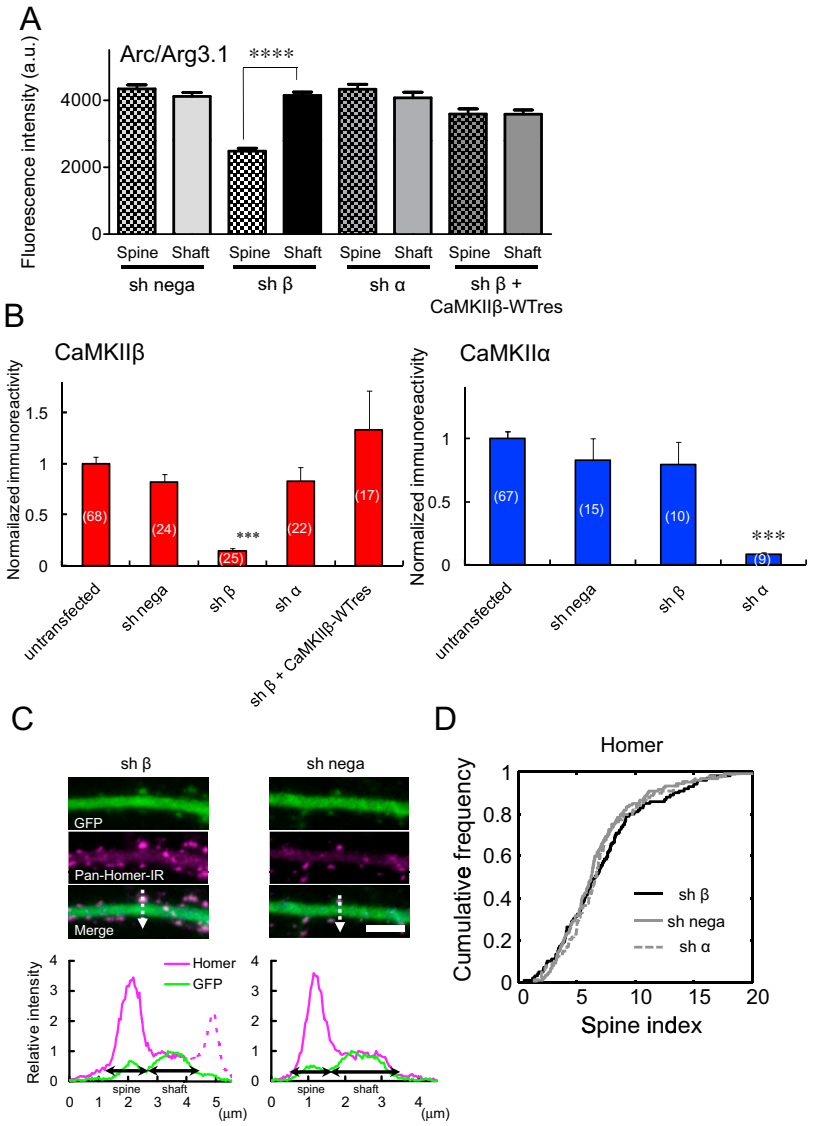

Figure S5. Additional Data and the Specificity of CaMKIIβ Knockdown Experiments, Related to Figure 5

(A) The average absolute intensities of Arc IR in the spines and shafts of shRNA-treated hippocampal neurons. The peak intensities of the spines and dendritic shaft were measured, and the average intensities within each condition are expressed as bars. The numbers of spines (n) and cells (N) analyzed were n = 275 (N = 36) for sh β, n = 218 (N = 30) for sh nega, n = 114 (N = 8) for sh α, and n = 148 (N = 11) for sh β + CaMKIIβ-WTres. The same dataset was used for calculation of the spine index shown in Figure 5C. ****$p < 0.0001$ by repeated ANOVA with a post hoc paired comparison. Note that the absolute levels in the spines and shafts, as shown in this panel, are to be distinguished from those in the PSD and shaft, as were shown in Figures S2D and S3C. The definition of fluorescent intensities was distinct both in terms of ROIs (PSD/nonPSD defined by PSD-95 IR versus spine/shaft defined by the line profile) and parameters used (averaged versus peak intensities), thus resulting in a slightly different, yet generally concordant, representation of Arc synaptic accumulation.

(B) The specificity and efficiency of the shRNA-based CaMKII knockdown. Hippocampal neurons transfected with shRNA vectors were immunostained, and the average immunofluorescence intensity of the cell body was measured and averaged across neurons. The IRs were background subtracted and normalized with the value of untransfected neurons. Left: CaMKIIβ expression levels. Specific CaMKIIβ knockdown was observed with sh β, but not sh nega or sh α, demonstrating the specificity of the RNAi-knockdown. Cotransfection of an RNAi-resistant wild-type CaMKIIβ expression vector and the sh β plasmid resulted in the full recovery of CaMKIIβ expression levels. The numbers of cells (N) examined were untransfected (N = 68), sh nega (N = 24), sh β (N = 25), sh α (N = 22), and sh β + CaMKIIβ-WTres (N = 17). Right: CaMKIIα expression levels. Specific CaMKIIα knockdown was observed with sh α, but not sh β, demonstrating the specificity of the RNAi. Numbers of cells (N) examined were untransfected (N = 67), sh nega (N = 15), sh β (N = 10), and sh α (N = 9). Asterisks represent significant differences between groups by ANOVA with a post hoc Tukey's test compared to the untransfected control (***$p < 0.001$).

(C and D) CaMKIIβ knockdown has no effect on synaptic Homer concentrations. (C) Representative images of Homer accumulation in the dendritic spines of neurons transfected with sh RNA vectors. Line profiles of IR revealed no apparent effect of CaMKIIβ knockdown on Homer spine accumulation. Scale bar, 5 μm. (D) The cumulative frequency of the spine index of Homer. No statistical differences were detected between the three conditions. The numbers of spines (n) and cells (N) analyzed were n = 99 (N = 7) for sh β, n = 120 (N = 7) for sh nega, and n = 88 (N = 8) for sh α.

Error bars represent SEM.

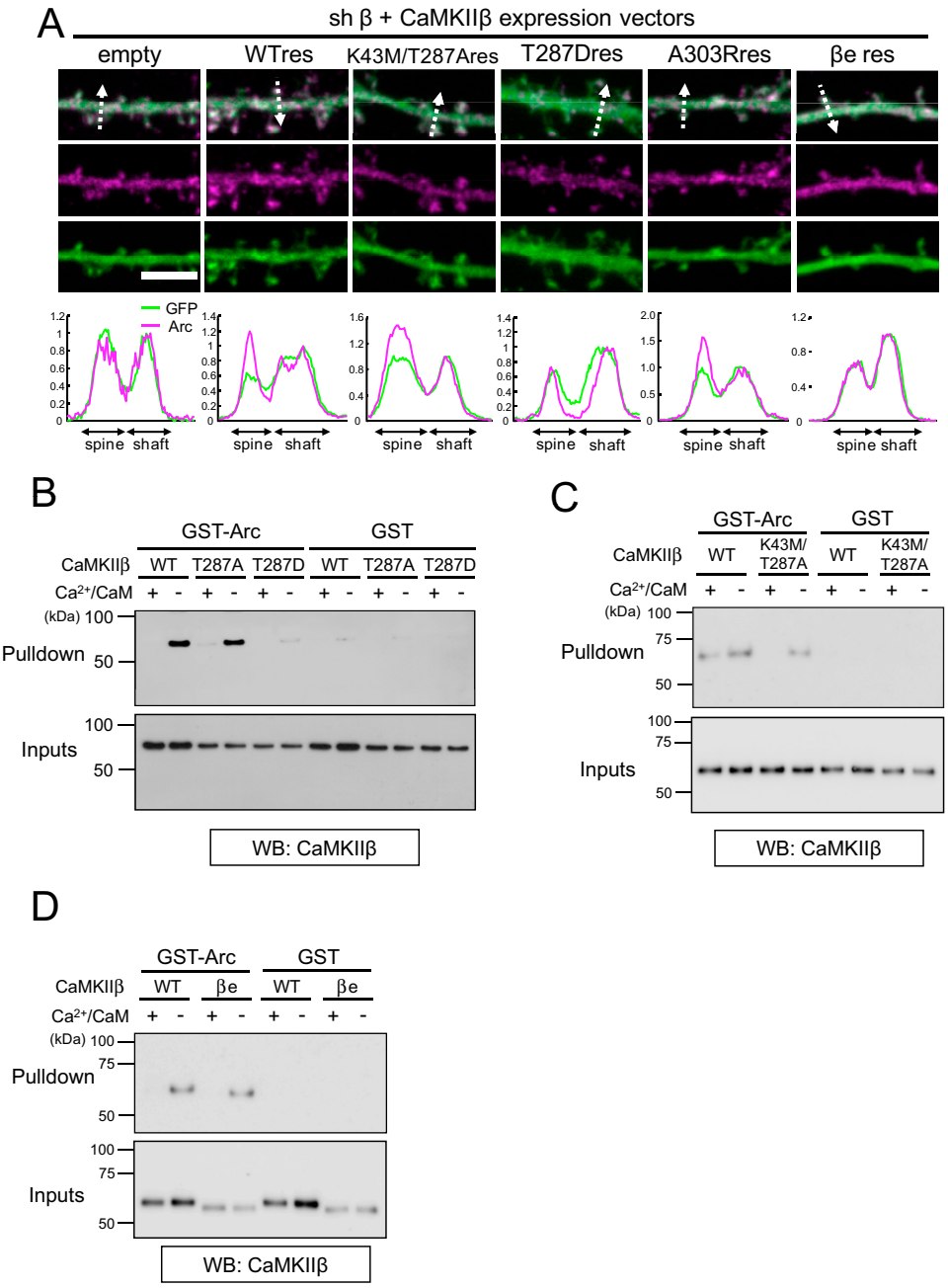

Figure S6. Effects of RNAi-Resistant CaMKIIβ Mutant Expression on Arc Synaptic Localization in CaMKIIβ Knockdown Neurons and Binding Abilities of CaMKIIβ Mutants to Arc, Related to Figure 5

(A) Representative dendritic segments of shRNA-CaMKIIβ knockdown neurons with RNAi-resistant CaMKIIβ expression. Immunostained dendrites and line-profiles were shown as in Figure 5. empty, empty expression vector only; WT, wild-type; K43M/T287A, kinase-dead and autophosphorylation-deficient; T287D, phospho-mimic/constitutively active; A303R, CaM-binding deficient; βe, F-actin-binding deficient; "res" in each label represents RNAi-resistant. Scale bar, 5 μm.

(B) GST-pull-down assay of phospho-mimic, constitutively active T287D and autophosphorylation-deficient T287A mutants of CaMKIIβ. The T287D mutant showed very weak binding, whereas the T287A mutant and wild-type CaMKIIβ showed comparable Arc binding in the absence of Ca^{2+} and CaM.

(C) GST-pull-down assay of a kinase-dead/autophosphorylation-deficient K43M/T287A mutant of CaMKIIβ showing Arc binding in the absence of Ca^{2+} and CaM as wild-type.

(D) GST-pull-down assay of a non-F-actin binding CaMKIIβe isoform showing Arc binding in the absence of Ca^{2+} and CaM as wild-type.

WB, western blot.

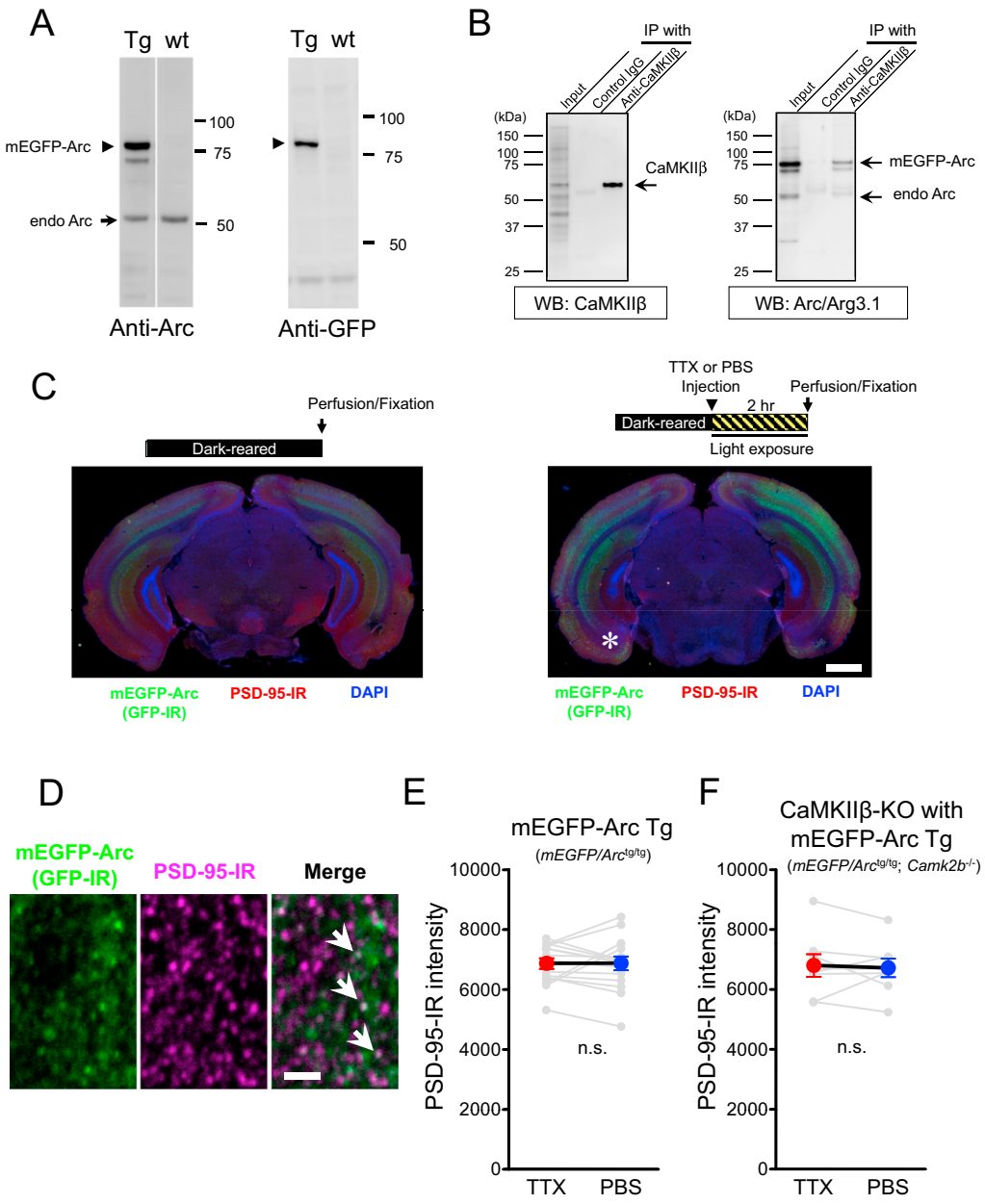

Figure S7. Activity-Induced mEGFP-Arc in Tg Mice and Additional Controls for Synaptic Accumulation of mEGFP-Arc In Vivo, Related to Figure 6

(A) Transgene expression in mEGFP-Arc Tg mice. Lysates were prepared from the neocortex of mEGFP-Arc Tg mice and wild-type (wt) control mice and then subjected to Western blotting with anti-Arc and anti-GFP antibodies. A specific band of the expected molecular weight of the transgene product was detected.

(B) Brain co-immunoprecipitation showing that mEGFP-Arc protein also interacts with CaMKIIβ. RIPA-buffer extracted brain lysates were prepared from mEGFP-Arc Tg mice, immunoprecipitated with an anti-CaMKIIβ antibody and probed with the anti-CaMKIIβ or anti-Arc antibody. The CaMKIIβ immunoprecipitates contained both endogenous Arc and the transgene product, mEGFP-Arc. IP, immunoprecipitation; WB, western blot.

(C) Representative immunohistochemical images of Tg mice underwent different sensory experiences and ocular TTX injection. Schematic paradigms are shown at the top of each image. Brain sections of the mouse visual cortex were immunostained with anti-GFP antibody (for mEGFP-Arc) and PSD-95. Left: little mEGFP-Arc expression was observed in the visual cortex under the dark-rear condition. Right: light exposure induced robust mEGFP expression in the visual cortex of the control hemisphere whereas the transgene induction was effectively blocked by monocular TTX injection (Asterisk). Scale bar, 1mm.

(D) Representative high-power images of mEGFP-Arc and PSD-95 IR in a section of the visual cortex. Similar images were used for the measurement of mEGFP-Arc signals in the PSD-95 spots. Arrows indicate spots with both mEGFP-Arc and PSD-95 IR. Scale bar, 2 μm.

(E) The intra-animal comparison of PSD-95 IR in the ROIs used for mEGFP-Arc quantification in Figure 6D. No difference was detected (N = 15 animals).

(F) No interhemispheric differences in PSD-95-IR levels were detected in the ROIs used for the analysis shown in Figure 6E (N = 8 animals).

Error bars represent SEM. n.s., not significant.